

The Experimental Status of Glueballs

C. A. Meyer¹ and V. Crede²

¹Carnegie Mellon University, Pittsburgh, PA 15213 USA

¹Florida State University, Tallahassee, FL 32306 USA

June 22, 2008

Abstract

1 Introduction

While we believe that Quantum Chromodynamics (QCD) is the correct description of the interactions of quarks and gluons, it is a theory that is very difficult to solve in the low-energy regime—that which describes the particles of which the universe is made. This is changing with advances that have been made in Lattice QCD, and the access to ever faster computers. Within QCD, one of the perplexing issues has been the existence of gluonic excitations. In the meson sector, nearly all the observed states can be explained as simple $q\bar{q}$ systems, with the naive quark model both providing a very good explanations for these particles, as well as providing a nice framework in which they can be described.

However, both phenomenological models and lattice calculations predict that there should exist additional states in which the gluons themselves can contribute to the quantum numbers of the states. These include the pure-gluon states known as glueballs as well as $q\bar{q}$ states with explicit glue, known as hybrid mesons. Some of these latter states are expected to have quantum numbers which are forbidden to $q\bar{q}$ systems—exotic quantum numbers which can provide a unique signature for the existence of such particles.

Over the last decade, a great deal of new experimental data on mesons has been collected. This new information bears directly on both the search for, and our current understanding of gluonic excitations of mesons, in particular glueballs and hybrids. In this review, we will focus on glueballs, rather than gluonic excitations in general. This paper will review the new data, and present a sampling of the phenomenological work that has been developed based on this.

In order to be able to discuss glueballs, it is necessary to understand conventional quark-antiquark systems (mesons). Over the last decade, there have been several relevant reviews on this subject, all of which touch upon gluonic excitations at some level. Much of the newest data on mesons came from the Crystal Barrel experiment [1], and an excellent review on

the results of that experiment can be found in reference [2]. In addition to this, a review on spectroscopy can be found in reference [3]. Reference [4] is a review on *gluonic hadrons* from about the same time. A more recent review on the mesons beyond the naive quark model can be found in reference [5]. Most recently is an encyclopedic review on meson spectroscopy and gluonic excitations which can be found in reference [6]. Finally, many useful mini-reviews can be found in the *Review of Particle Physics* [7].

2 Meson Spectroscopy

Before discussing the expectations for gluonic excitations, we will briefly discuss the simple quark model picture for mesons. A meson consists of a $q\bar{q}$ system, which because it contains both a particle and an antiparticle, has intrinsic negative parity, $P = -1$. The total parity of such a system is given as $P = -(-1)^L$, where L is the orbital angular momentum in the $q\bar{q}$ system. Because quarks have spin $\frac{1}{2}$, the total spin of such a system can be either $S = 0$ or $S = 1$, which leads to a total angular momentum $J = L + S$, where the sum is made according to the rules of addition for angular momentum. In addition the parity, there is also C-parity, or charge conjugation, which for a $q\bar{q}$ system is $C = (-1)^{L+S}$.

The two lightest quarks also carry an additional quantum number: isospin. Each has total isospin $\frac{1}{2}$, with the u quark being the $+\frac{1}{2}$ part and the d quark being the $-\frac{1}{2}$ part of the doublet. If we form a meson out of only these, we can have $I = 0$ or $I = 1$. If one of the quarks is a strange quark, then $I = \frac{1}{2}$ and if both are strange, then $I = 0$. For a $q\bar{q}$ system, we can define an additional conserved quantum number, G-parity: $G = (-1)^{L+S+I}$. Using these relationships to build up possible $\mathbf{J}^{\mathbf{PC}}$'s for mesons, we find that the following quantum numbers are allowed:

$$0^{-+}, 0^{++}, 1^{--}, 1^{+-}, 1^{-+}, 2^{--}, 2^{+-}, 2^{++}, 3^{--}, 3^{+-}, 3^{-+}, \dots \quad (1)$$

and looking carefully at these, we find that there is a sequence of $\mathbf{J}^{\mathbf{PC}}$'s which are not allowed for a simple $q\bar{q}$ system.

$$0^{--}, 0^{+-}, 1^{++}, 2^{+-}, 3^{++}, \dots \quad (2)$$

These latter quantum numbers are known as *explicitly exotic* quantum numbers and if observed, would correspond to something beyond the simple $q\bar{q}$ states of the quark model.

If we now consider only the three lightest quarks, u , d and s then we can form 9 $q\bar{q}$ combinations, all of which can have the same S , L and J . We can represent these in spectroscopic notation, $^{2S+1}L_J$, or as states of total spin, parity and for the neutral states, charge conjugation: J^{PC} . Naively, these $q\bar{q}$ combinations would simply be a quark and an antiquark. However, those states consisting of the same quark and antiquark ($u\bar{u}$, $d\bar{d}$ and $s\bar{s}$) are rotated into three other states based on Isospin and SU(3) symmetries. The combinations shown in equation 3 correspond to the non-zero isospin states, while those in equation 4 correspond to a pair of isospin zero states. The latter two states are also mixed

by SU(3) to yield a singlet ($|1\rangle$) and octet ($|8\rangle$) state.

$$\begin{array}{ccc} & (d\bar{s}) & (u\bar{s}) \\ (d\bar{u}) & \frac{1}{\sqrt{2}}(u\bar{u} - d\bar{d}) & (u\bar{d}) \\ & (s\bar{d}) & (s\bar{u}) \end{array} \quad (3)$$

$$|8\rangle = \frac{1}{\sqrt{6}}(u\bar{u} + d\bar{d} - 2s\bar{s}) \quad |1\rangle = \frac{1}{\sqrt{3}}(u\bar{u} + d\bar{d} + s\bar{s}) \quad (4)$$

The nominal mapping of these states onto the familiar pseudoscalar mesons is shown in 5 and 6.

$$\begin{array}{ccc} & K^0 & K^+ \\ \pi^- & \pi^0 & \pi^+ \\ & \bar{K}^0 & K^- \end{array} \quad (5)$$

$$\eta \quad \eta' \quad (6)$$

However, because SU(3) is broken, the two $I = 0$ mesons in a given nonet are usually admixtures of the singlet ($|1\rangle = \frac{1}{\sqrt{3}}(u\bar{u} + d\bar{d} + s\bar{s})$) and octet ($|8\rangle = \frac{1}{\sqrt{6}}(u\bar{u} + d\bar{d} - 2s\bar{s})$) states. In nature, the physical states are mixtures, where the degree of mixing is given by an angle θ .

$$f = \cos\theta|1\rangle + \sin\theta|8\rangle \quad (7)$$

$$f' = \cos\theta|8\rangle - \sin\theta|1\rangle \quad (8)$$

For the vector mesons, ω and ϕ , one state is nearly pure light-quark ($n\bar{n}$) and the other is nearly pure $s\bar{s}$. This is known as ideal mixing and occurs when $\tan\theta = \frac{1}{\sqrt{2}}$. In Table 1 are listed our current picture of the ground state mesons for several different L 's. The last two columns list the linear (equation 9) and quadratic (equation 10) calculations of the mixing angle for the nonets.

$$\tan\theta = \frac{4m_K - m_a - 3m_{f'}}{2\sqrt{2}(m_a - m_K)} \quad (9)$$

$$\tan^2\theta = \frac{4m_K - m_a - 3m_{f'}}{-4m_K + m_a + 3m_f} \quad (10)$$

The mixing angle θ can also be used to compute relative decay rates to final states such as pairs of pseudoscalar mesons, or two-photon widths, for the f and f' in a given nonet. Examples of this can be found in reference [8] and reference therein. The key feature is that for a given nonet, the f and f' states can be identified by looking at the relative decay rates to pairs of particles.

The data are taken from the Particle Data Book [7].

As an example of a decay calculation, we consider the decay of the tensor ($J^{PC} = 2^{++}$) mesons to pairs of pseudoscalar mesons ($\pi\pi$, $K\bar{K}$ and $\eta\eta$). Following the work in references [8–10], we can compute a decay constant γ from the SU(3) algebra corresponding to the decays. This can then be turned into a decay rate, Γ as in equation 11

$$\Gamma = \gamma^2 \cdot f_L(q) \cdot q \quad (11)$$

$n^{2s+1}l_J$	J^{PC}	$I = 1$ $u\bar{d}\dots$	$I = \frac{1}{2}$ $u\bar{s}\dots$	$I = 0$ f	$I = 0$ f'	θ_q	θ_l
1^1S_0	0^{-+}	π	K	η	η'	-11.5°	-24.6°
1^3S_1	1^{--}	ρ	K^*	ω	ϕ	38.7°	36.0°
1^1P_1	1^{+-}	$b_1(1235)$	K_{1B}	$h_1(1170)$	$h_1(1380)$	29.6°	28.0°
1^3P_0	0^{++}	$a_0(1450)$	$K_0^*(1430)$	$f_0(1370)$	$f_0(1710)$		
1^3P_1	1^{++}	$a_1(1260)$	K_{1A}	$f_1(1285)$	$f_1(1420)$		
1^3P_2	2^{++}	$a_2(1320)$	$K_2^*(1430)$	$f_2(1270)$	$f_2'(1525)$		
1^1D_2	2^{-+}	$\pi_2(1670)$	$K_2(1770)$	$\eta_2(1645)$	$\eta_2(1870)$	32.0°	31.0°
1^3D_1	1^{--}	$\rho(1700)$	$K^*(1680)$	$\omega(1650)$			
1^3D_2	2^{--}		$K_2(1820)$				
1^3D_3	3^{--}	$\rho_3(16900)$	$K_3^*(1780)$	$\omega_3(1670)$	$\phi_3'(1850)$		
1^1F_4	4^{++}	$a_4(2040)$	$K_4^*(2045)$	$f_4(2050)$			
1^3G_5	5^{--}	$\rho_5(2350)$					
1^3H_6	6^{++}	$a_6(2450)$		$f_6(2510)$			
2^1S_0	0^{-+}	$\pi(1300)$	$K(1460)$	$\eta(1295)$	$\eta(1475)$	-22.4°	-22.6°
2^3S_1	1^{--}	$\rho(1450)$	$K^*(1410)$	$\omega(1420)$	$\phi(1680)$		

Table 1: A modified reproduction of the table from the 2006 Particle Data Book [8] showing the current assignment of known mesons to quark-model states. When sufficient states are know, the nonet mixing angle is computed using both the quadratic and linear forms.

where q is the break-up momentum of the meson into the pair of daughter mesons. amplitude γ depends on the nonet mixing angle and the psuedoscalar mixing angle, θ_P . A typical example is shown in Figure 1 which is shown in terms of an arbitrary scale factor. The quantitiy f_L is a form factor that depends on the angular momentum, L , between the pair of daughter mesons. A typical form is given as in equation 12

$$f_L(2) = q^{2L} e^{-\frac{q^2}{8\beta^2}} \quad (12)$$

where β is a constant that is in the range of 0.4 to 0.5 GeV/c. One can fit the ratio of decay rates to pairs of mesons for both the $f_2(1270)$ and the $f_2'(1525)$ and fit to the best value of the nonet mixing angle. We can compute a χ^2 between the measured and predicted decay rates to determine what the optimal choice of the mixing angle is. This is shown in Figure 2,

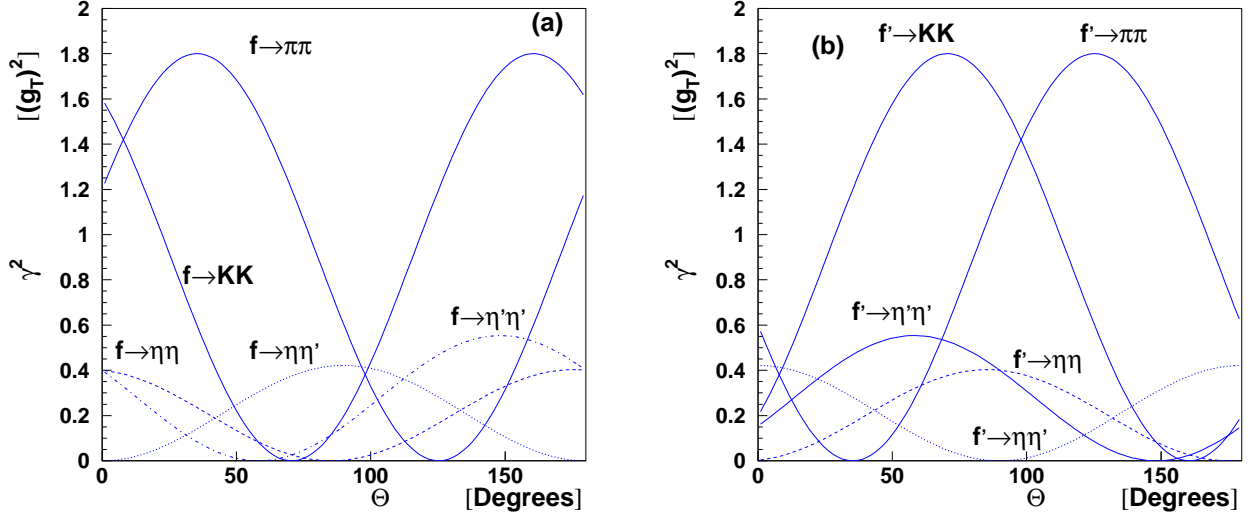


Figure 1: The decay amplitude, γ^2 , as a function of the nonet mixing angle, θ . (a) is for f decays while (b) is for f' decays. In this particular example, the pseudoscalar mixing angle is taken as $\theta_P = -17^\circ$.

where the optimal value is at about 32.5° . The location of the optimum does not depend strongly on either θ_P or β and is in good agreement with the values from the mass formulas for the tensors in Table 1.

Measuring the masses and decay rates of mesons can be used to identify the quark contents of a particular meson. The lightest glueballs have J^{PC} quantum numbers of normal mesons and would appear as an SU(3) singlet state. If they are near a nonet of the same J^{PC} quantum numbers, then they will appear as an extra f -like state. While the fact that there is an extra state is suggestive, the decay rates are also needed to unravel the quark content of the observed mesons.

3 Theoretical Expectations for Glueballs

3.1 Historical

One of the earliest models in which glueball masses were computed is the bag model [11]. In these early calculations, boundary conditions were placed on gluons confined inside the bag [12]. The gluon fields could be in transverse electric (TE) or transverse magnetic modes (TM). For a total angular momentum (J), the TE modes had parity of $(-1)^{(J+1)}$, while the TM modes had parity $(-1)^J$. The gluons then had to populate the bag to yield a color singlet state. This led to predictions for two- and three-gluon glueballs as given in Table 2.

Because glueballs contained no quarks, the expectation was that they would couple to all

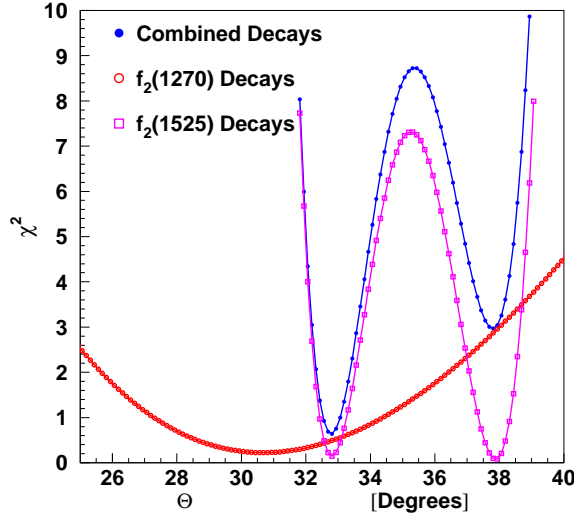


Figure 2: (color online) The χ^2 computed between the measured and predicted decay rates for the isoscalar tensor mesons. The open red circles are for the $f_2(1270)$ alone. The open purple squares are for the $f_2(1525)$ alone and the solid blue circles are for the combined fit. The former two are for one degree of freedom, while the latter is for three.

Gluons	J^{PC} Quantum Numbers	Mass
$(TE)^2$	$0^{++}, 2^{++}$	$0.96 \text{ GeV}/c^2$
$(TE)(TM)$	$0^{-+}, 1^{-+}, 2^{-+}$	$1.29 \text{ GeV}/c^2$
$(TE)^3$	$0^{+-}, 1^{++}, 2^{+-}, 3^{++}$	$1.46 \text{ GeV}/c^2$
$(TM)^2$	$0^{++}, 2^{++}$	$1.59 \text{ GeV}/c^2$

Table 2: Masses of glue balls in the bag model [12].

flavors of quarks equally. In a simple SU(3) calculation, the γ^2 from equation 11 are given in Table 3. In addition to the decay predictions, there are reactions which are expected to be *glue rich*. The first of these is radiative decays of the J/ψ . Because the $c\bar{c}$ quarks have to

Decay	$\pi\pi$	$K\bar{K}$	$\eta\eta$	$\eta\eta'$	$\eta'\eta'$
γ^2	3	4	1	0	1

Table 3: The expected decay amplitudes for a glueball normalized to the rate to $\eta\eta$.

decay via annihilation, the intermediate state must gluons in it. This same argument can be applied to other $q\bar{q}$ reactions such as proton-antiproton annihilation and v decays. In the J/ψ decays, Chanowitz [13] proposed variable known as *stickiness* which is the relative rate of production of some hadron h in radiative J/ψ decays to its two-photon width (photons only couple to electric charge, hence to quarks). The stickiness, S can be defined as in equation 13

for a hadron h of mass $M(h)$. l is the lowest orbital angular momentum needed to couple to two vector particles and the photon energy k_γ is that from the radiative decay in the ψ rest frame. The overall constant C is chosen such that $S(f_2(1270)) = 1$.

$$S = C \left(\frac{M(h)}{k_\gamma} \right)^{2l+1} \frac{\Gamma(\psi \rightarrow \gamma h)}{\Gamma(h \rightarrow \gamma\gamma)} \quad (13)$$

While this quantity has been computed for many of the glueball candidates, it appears to be most limited by our detailed knowledge of the two-photon width of the states [14]. A recent analysis by Pennington [15] has looked closely at the world data for this and still finds sizeable uncertainties in these widths.

Related to stickiness, Farrar [16] proposed a method of extracting decay rate of hadrons to gluons based on the radiative decay rate of vector quarkonium to the state. This was later applied to several mesons by Close [17] to try and distinguish glueball candidates.

There has also been questions raised about the validity of the flavor-blind decay assumption of glueballs. Lee and Weingarten [18] looked at decays of glueballs and proposed that the decay rates should scale with the mass of the mesons, thus favoring the heaviest possible meson pairs. Close [17]

Particular excitement was raised over the very large production of a pseudoscalar state (now known as the $\eta(1405)$) in radiative J/ψ decays [19], [20], [21]. Mini-review in pdg [22].

Mini-review in pdg on scalars [23].

3.2 Model Calculations

The first glueball mass calculation within the fluxtube model was carried out by Isgur and Paton [24, 25]. In this model the glueball is treated as a closed fluxtube. Isgur and Paton found that the lightest glueball has $J^{PC} = 0^{++}$ and a mass of $1.52 \text{ GeV}/c^2$. In later flux-tube calculations [26], calculations were made for the lightest three glueball masses. These were found to be consistent with the lattice calculations in reference [27]. Table 4 summarizes several flux-tube calculations of the scalar, tensor and pseudoscalar glueball. Finally, a recent article speculates that within the flux tube model, the scalar and pseudoscalar glueball should be degenerate in mass [28].

$J^{PC} = 0^{++}$	$J^{PC} = 2^{++}$	$J^{PC} = 0^{-+}$
1.52 GeV/ c^2 [24, 25]	2.84 GeV/ c^2 [24, 25]	2.79 GeV/ c^2 [24, 25]
1.68 GeV/ c^2 [26]	2.69 GeV/ c^2 [26]	2.57 GeV/ c^2 [26]
1.6 GeV/ c^2 [29]		

Table 4: Fluxtube predictions for masses of the lowest lying glueballs.

Swanson and Szepeaniak compute the glueball spectrum in Hamiltonian QCD in the Coulomb Gauge [30] by constructing a quasiparticle gluon basis. They also find results which are in good agreement with lattice calculations. The lightest glueball is a scalar with mass of $1.98 \text{ GeV}/c^2$, followed by a pseudoscalar at $2.22 \text{ GeV}/c^2$ and then a tensor at $2.42 \text{ GeV}/c^2$.

3.3 *Lattice Calculations*

Lattice QCD discretizes space and time on a four-dimensional Euclidean lattice, and use this to solve QCD numerically. This is done by looking at path integrals of the action on the discrete lattice. Quarks and antiquarks live on the discrete points of the lattice, while gluons span the links between the points. Depending on the problem being solved, and the availability of computing resources, the size of the lattice may vary. In addition, there are many different choices for the action, each of which has its own advantages and disadvantages. In specifying the calculation, the grid and action are specified and a damping factor, β , is chosen. After the calculation has been completed, the physical quantities of interest as well as the lattice spacing can be determined. For a given choice of action, a larger β maps into a smaller lattice spacing. However, the same β with different actions can lead to quite different lattice spacings.

To date, most lattice calculations have been carried out in the quenched approximations, where the fluctuation of a gluon into a quark-antiquark pair is left out. As computer power continues to increase, and more efficient ways of carrying out calculations evolve, this is starting to change.

There is also a lattice artifact that can affect the mass calculations of the scalar glueball [31]. A singularity not related to QCD can cause the mass of the scalar glueball to be artificially small. This effect is particularly apparent when Wilson fermions are used with a too-large lattice spacing. Other choices are less sensitive to this, and when the lattice spacing is small enough, the effect does go away. However, for Wilson fermions, the critical value of β is 5.7, which is very close to the values used in many glueball calculations.

Some of the earliest lattice calculations of the glueball spectrum were carried out in the quenched approximation on relatively small lattices [32], [33]. These calculations indicated that the mass of the lightest glueball spectrum started at about 1.5 GeV/c². As the both computational resources increased and the lattice actions and methods improved, calculations on larger were carried out, and the spectrum of the states began to emerge [34]. After extrapolating to the continuum limit, the lightest three states emerge as the scalar ($J^{PC} = 0^{++}$), tensor ($J^{PC} = 2^{++}$) and the pseudoscalar ($J^{PC} = 0^{-+}$), with the scalar around 1.55 ± 0.05 GeV/c², the tensor at 2.27 ± 0.1 GeV/c² and the pseudoscalar at about the same mass. It was also possible to identify a number of other states with the first exotic (non- $q\bar{q}$) quantum number state above 3 GeV/c².

A later calculation using a larger lattice and smaller lattice parameters yielded a mass for the scalar glueball 1.625 ± 0.094 GeV/c² [35,36]. The authors also calculated the decay of the scalar glueball to pairs of pseudoscalar mesons and estimated that the total width of the glueball would be under 0.2 GeV/c². They also found that the decay width of the scalar glueball depended on the mass of the daughter mesons, with coupling increasing with mass. This was in contradiction to the lore that glueballs should decay in a flavor-blind fashion with the coupling to pairs of pseudoscalar mesons being independent of flavor or mass. Other work has followed this in discussions of violations of flavor-blind decays [37,38]. This breaking is (effectively) accomplished by introducing a parameter r in the matrix that mixes quarkonium with glueballs. For flavor blind decays, $r = 1$. Values that are close to 1 are

typically found. On the lattice [35,36], it is found that $r = 1.2 \pm 0.07$, while a fit to data [37] finds $r = 1 \pm 0.3$. Finally, in a microscopic quark/gluon model [38], $r = 1.1 - 1.2$. Taken together, one should probably expect small violations of flavor-blind decays for glueballs, but not large.

Improved action calculations [39], [40] is essentially the state of the art

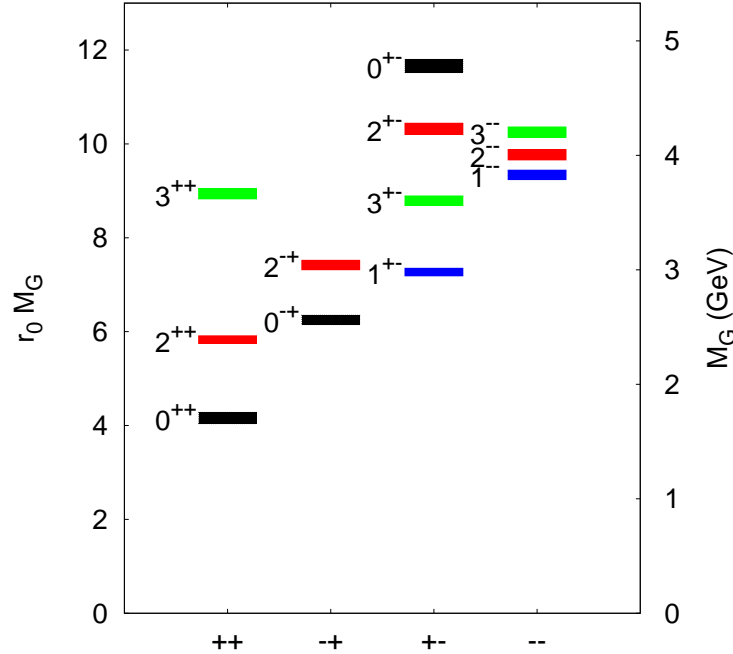


Figure 3: (color online) The mass spectrum of glueballs. The height of each box indicates the statistical uncertainty. Figure used with permission from reference [40].

Hart and Tepper [41] carried out an unquenched calculation of the scalar and tensor glueballs using Wilson fermions. They found that the tensor mass did not move, while the scalar mass came out at about 85% of the unquenched mass. McNeile [42] speculates that this may be a result of the lattice artifact mentioned above. In another unquenched calculation, Gregory [43], find that unquenching the lattice calculations for glueballs appears not to significantly alter the results from unquenched calculations.

4 The Known Mesons

4.1 Experimental Methods and Major Experiments

Results on meson spectroscopy have come from a large variety of experiments using different experimental techniques. Production of glueballs has mainly been predicted for glue-rich environments []. The most promising examples are proton-antiproton annihilation or radiative decays of quarkonia, where one of the three gluons arising from the quark-antiquark

J^{PC}	M_G (GeV/c ²)
0^{++}	1.710(.050)(.080)
2^{++}	2.390(.030)(.120)
0^{-+}	2.560(.035)(.120)
1^{+-}	2.980(.030)(.140)
2^{-+}	3.040(.040)(.150)
3^{+-}	3.600(.040)(.170)
3^{++}	3.670(.050)(.180)
1^{--}	3.830(.040)(.190)
2^{--}	4.010(.045)(.200)
3^{--}	4.200(.045)(.200)
2^{+-}	4.230(.050)(.200)
0^{+-}	4.780(.060)(.230)

Table 5: The glueball mass spectrum in physical units. For the mass of the glueballs (M_G), the first error comes from the combined uncertainty of $r_0 M_G$, the second from the uncertainty of $r_0^{-1} = 410(20)$ MeV

annihilation is replaced by a photon leaving two gluons to form bound states. The following sections describe the main experimental methods and major experiments devoted to the study of meson resonances and the search for glueballs.

Proton-Antiproton Annihilation

In $p\bar{p}$ annihilations, glueballs may be formed when quark-antiquark pairs annihilate into gluons. Though not very likely, this may proceed via *formation* (as opposed to *production*) without a recoil particle; in this case, exotic quantum numbers are forbidden and the properties of the glueball candidate can be determined from the initial state. Instead, production of a heavier resonance recoiling against another meson is normally expected, but interaction of gluons forming glueballs sounds likely. However, the usually observed final states consisting of light u- and d-quarks can be just as effectively produced by quark rearrangements, i.e. without glueballs in the intermediate state. In $p\bar{p}$ annihilations at rest, mesons with masses up to 1.7 GeV/c² can be produced. [Feynman Graphs of \$p\bar{p}\$ formation, production, etc.?](#)

The $p\bar{p}$ annihilation at rest offers a natural way of limiting the number of partial waves involved in the process facilitating spin-parity analyses. At the Low-Energy Antiproton Ring (LEAR) at CERN, slow antiprotons of about 200 MeV/c were decelerated in liquid or gaseous hydrogen (or deuterium) by ionizing hydrogen molecules and eventually stopped and captured by protons forming hydrogen-like atoms called *protonium*. A highly excited $p\bar{p}$ state is formed by ejecting an electron via *Auger effect*:

$$\bar{p} + \text{H}_2 \rightarrow \boxed{p\bar{p}} + \text{H} + \text{e}^-$$

Annihilation takes place from atomic orbits. The capture of the \bar{p} typically occurs at a principal quantum number of $n \approx 30$ and at a high angular momentum between the proton

and the antiproton of $L \approx n/2$. For $n \approx 30$, the radius of the protonium atom matches the size of hydrogen atoms in their ground state. For lower n values, the protonium radius becomes much smaller; the first Bohr radius of the $p\bar{p}$ atom is 57 fm. Due to this small size and due to the fact that protonium carries no charge, it can diffuse through hydrogen molecules. The \bar{p} reaches an atomic state with angular momentum $L = 0$ or $L = 1$ when annihilation takes place. In media of high density like liquid H_2 , the protonium is exposed to extremely large electromagnetic fields so that rotation invariance is broken. Transitions between different nearly mass-degenerate angular momentum states at the same high principal quantum number n occur (*Stark mixing*). The effect is proportional to the target density and for liquid targets the rate is very high, such that about 90 % of all annihilations appear to be S-wave annihilations. For gaseous hydrogen targets, the P-wave contribution is much larger. The incoherent superposition of the $L = 0$ or $L = 1$ angular momentum eigenstates of the $p\bar{p}$ atom corresponds to six different partial waves: $^1S_0, ^3S_1, ^1P_1, ^3P_0, ^3P_1, ^3P_2$.

Proton and antiproton both carry isospin $|I, I_3\rangle = |\frac{1}{2}, \pm\frac{1}{2}\rangle$ and can couple to either $|I = 0, I_3 = 0\rangle$ or $|I = 1, I_3 = 0\rangle$. Given that initial state interactions due to $p\bar{p} \rightarrow n\bar{n}$ are small [44], we have

$$p\bar{p} = \sqrt{\frac{1}{2}}(|I = 1, I_3 = 0\rangle + |I = 0, I_3 = 0\rangle). \quad (14)$$

A large number of meson resonances was studied in $\bar{p}N$ annihilations at rest and in flight. The most recent experiments were carried out at LEAR at CERN; the accelerator was turned off in 1996. The OBELIX Collaboration at LEAR had a dedicated program on light-meson spectroscopy. The detector system allowed operation of a variety of hydrogen targets: liquid H_2 , gaseous H_2 at normal temperature and pressure, and also a target at very low pressures. A special feature of the detector was the possibility to study antineutron interactions, where the \bar{n} beam was produced by charge exchange in a liquid H_2 target. The Open Axial-Field Magnet of the experimental setup provided a magnetic field of 0.5 T. Particle detection proceeded via a Spiral Projection Chamber acting as vertex detector, a time-of-flight (TOF) system, a Jet Drift Chamber (JDC) for tracking and identification of charged particles by means of dE/dx , and a High-Angular Resolution Gamma Detector (HARGD), a system of four supermodules for the identification and measurement of neutral annihilation products. A detailed description of the experimental setup is given in [45]. The resolution of pions in the reaction $p\bar{p} \rightarrow \pi^+\pi^-$ was determined to 3.5 % at 928 MeV/ c and the mass resolution of π^0 mesons given by $\sigma = 10 \text{ MeV}/c^2$. Results are summarized in [45–52].

Adjacent to OBELIX in the experimental hall, the Crystal Barrel spectrometer was operational from 1989-1996. The apparatus is described in [1] and shown in Fig. 4. It could measure multi-meson final states including charged particles and photons from the decay of neutral mesons. From the inside target to the outside magnet surrounding all components of the experiment, the detector consisted of two concentric cylindrical multi-wire proportional chambers (PWC), a jet drift chamber (JDC), and a barrel-shaped, modular electromagnetic CsI(Tl) calorimeter giving the detector system its name. The PWC was replaced by a silicon vertex detector in September 1995. The JDC had 30 sectors with each

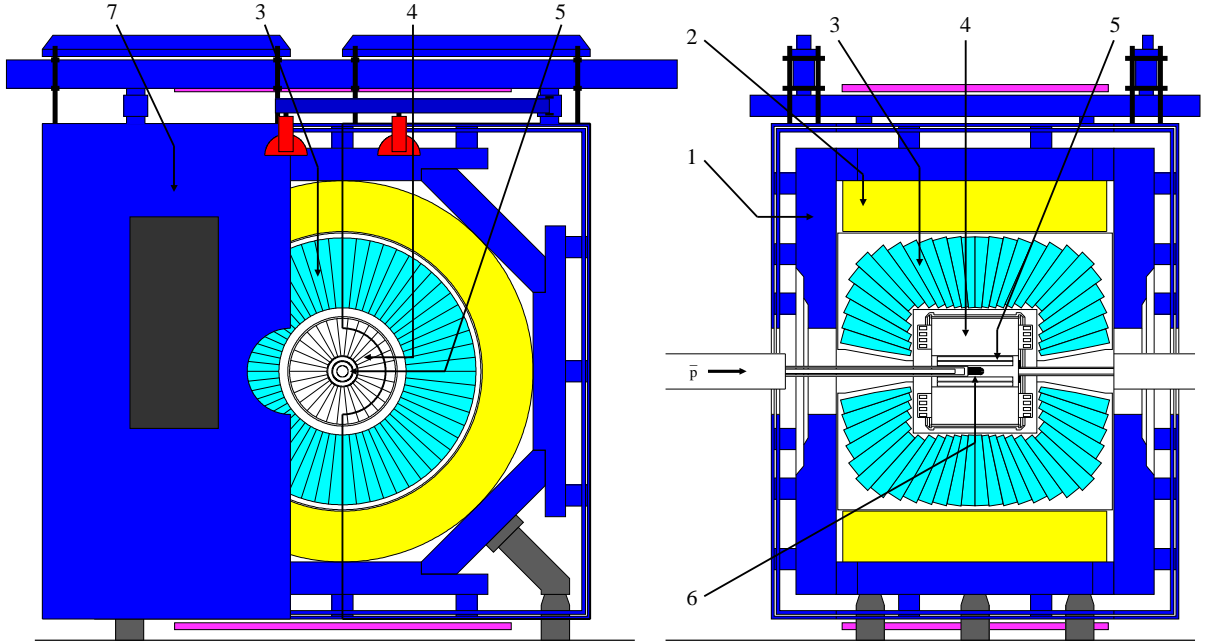


Figure 4: Cross section of the Crystal-Barrel Detector at LEAR. From the outside: (1) magnet yoke, (2) magnet coils, (3) CsI(Tl) barrel calorimeter, (4) jet drift chamber, (5) proportional wire chamber, (6) target, (7) one half of the endplate

sector having 23 sense wires and allowed the detection and identification of charged particles with a momentum resolution for pions of less than 2 % at 200 MeV/c. Separation of π/K below 500 MeV/c proceeded via ionisation sampling. The magnetic field of up to 1.5 T with a relative homogeneity of 2 % in the region of the drift chamber was created by a conventional solenoid ($B_r \approx B_\phi \approx 0$, $B_z \neq 0$) which was encased in a box-shaped flux return yoke. Data were taken on hydrogen and deuterium at rest [53–71] and at different incident beam momenta [72–76].

e^+e^- Annihilation Experiments and Radiative Decays of Quarkonia

The study of radiative decays of quarkonia is considered most suggestive in the glueball search. Most of the information in this field has centered on J/ψ decays; after photon emission, the $c\bar{c}$ annihilation can go through C -even gg states, and hence may have a strong coupling to the low-lying glueballs. Study of J/ψ decays facilitates the search because the $D\bar{D}$ threshold is above the J/ψ mass of 3097 MeV/ c^2 and the OZI rule¹ suppresses decays of the $c\bar{c}$ system into light quarks. Radiative $\Upsilon(1S)$ decays are also supposed to be glue-rich and a corresponding list of two-body decay branching ratios for $\Upsilon(1S)$ is desirable. Results have been recently reported by the CLEO Collaboration [77, 78]. The search for glueballs in

¹The OZI rule states that decays corresponding to disconnected quark diagrams are forbidden.

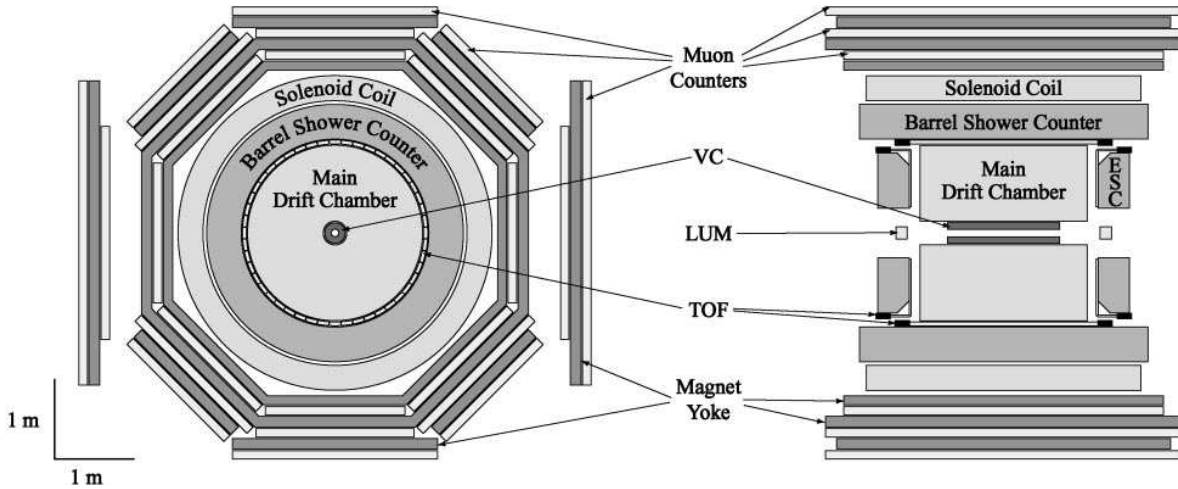


Figure 5: End view (left) and side view (right) of the BES-II detector at IHEP, Beijing

$\Upsilon(1S)$ decays is however challenging because the ratio:

$$\frac{\Gamma_{\Upsilon}^{\text{rad}}}{\Gamma_{\Upsilon}^{\text{tot}}} = \left(\frac{\alpha_s(\Upsilon)}{\alpha_s(J/\psi)} \right)^4 \left(\frac{\Gamma_{\Upsilon \rightarrow e^+e^-}}{\Gamma_{\Upsilon}^{\text{tot}}} \cdot \frac{\Gamma_{J/\psi}^{\text{tot}}}{\Gamma_{J/\psi \rightarrow e^+e^-}} \cdot \frac{\Gamma_{J/\psi}^{\text{rad}}}{\Gamma_{J/\psi}^{\text{tot}}} \right) \approx 0.013 \quad (15)$$

is much smaller than for J/ψ mesons and a naive suppression factor of ~ 6 is expected. Moreover, information on any possible χ_{cJ} hadronic decays provides valuable insight into possible glueball dynamics.

J/ψ decays can also be used to study the flavor content of mesons in the so-called *flavor-tagging* approach. The reaction $J/\psi \rightarrow V X$ may serve as an example, where V is one of the light vector mesons (ω, ϕ, ρ^0) and X is the exclusive final state of interest. The flavor of X can now be tagged as the structure of the light vector is known. If the $\phi(1020)$ is produced, for instance, then the reaction $J/\psi \rightarrow \phi X$ indicates those recoiling mesons X , which are produced through their $s\bar{s}$ component. For this reason, J/ψ decays to $\omega f_2(1270)$ and $\phi f_2'(1525)$ are clearly observed, but decays to $\omega f_2'(1525)$ and $\phi f_2(1270)$ are missing. High-statistics flavor-tagging is a promising tool and has helped determine mixing angles as discussed in section 2. Similar decays of the $\psi'(3770)$, the first radial excitation of the J/ψ , provides access to mesons with even higher masses.

Radiative decays of $c\bar{c}$ states can best be studied in *formation* at e^+e^- colliders via a virtual photon in the process:

$$e^+e^- \rightarrow \gamma^* \rightarrow c\bar{c}. \quad (16)$$

Only states with the quantum numbers of the photon ($J^P = 1^-$) can be created and the lowest-mass candidate is the 1^3S_1 - J/ψ state.

Several reactions have been studied in the BES experiment at the e^+e^- collider BEPC at IHEP, Beijing. Operation started in 1989 with a maximum collider energy of $2E = 4.4$ GeV and a luminosity of up to $10^{31}/\text{cm}^2/\text{s}$. A layout of the BES-II detector is shown in Fig. 5. The detector is a large solid-angle magnetic spectrometer based on a conventional 0.4 T solenoidal magnet [79]. It identifies charged particles using dE/dx measurements in the drift chambers and time-of-flight measurements in a barrel-like array of 48 scintillation counters. The barrel shower counter measures the energy of photons with a resolution of $\sigma_E/E = 28\%/\sqrt{E}$ (E in GeV). More than 10^7 J/ψ events and more than 10^6 $\psi'(3770)$ events have been accumulated. The BES-III detector is a major upgrade aiming at $L = 10^{33}/\text{cm}^2/\text{s}$ luminosity and recorded its first hadronic event in July 2008. Results relevant to this review are summarized in [80–86].

Radiative decays of $c\bar{c}$ and Υ ($b\bar{b}$) states have been studied with the CLEO detector at the e^+e^- collider CESR at Cornell University. Based on the CLEO-II detector, the CLEO-III detector started operation in 1999 [87]. CLEO consisted of drift chambers for tracking and dE/dx measurements and a CsI electromagnetic calorimeter based on 7800 modules inside a 1.5 T magnetic field. For CLEO-III, a silicon-strip vertex detector and a ring-imaging Čerenkov detector for particle identification were added. The integrated luminosity accumulated by the CLEO-III detector in 1999–2003 was 16 fb^{-1} . In 2003, CLEO was upgraded to CLEO-c in order to study charm physics at high luminosities. The CLEO-c operations finally ended in Spring 2008. The anticipated program of collecting data at $\sqrt{s} \sim 3.10$ GeV for the J/ψ was given up due to technical difficulties in favor of a total of 572 pb^{-1} on the $\psi'(3770)$. Selected results of the CLEO Collaboration can be found in [77, 78, 88–90].

The KLOE Collaboration has studied radiative $\phi(1020)$ decays to $f_0(980)$ and $a_0(980)$ at the Frascati ϕ factory DAPHNE. These decays play an important role in the study of the controversial structure of the light scalar mesons. In particular, the ratio $\mathcal{B}(\phi \rightarrow f_0(980)\gamma)/\mathcal{B}(\phi \rightarrow a_0(980)\gamma)$ depends strongly on the structure of the scalars [91]. The KLOE detector consists of a cylindrical drift chamber, which is surrounded by an electromagnetic calorimeter and a superconducting solenoid providing a 0.52 T magnetic field. The energy resolution of the calorimeter is $\sigma_E/E = 5.7\%/\sqrt{E}$ (E in GeV). The detector accumulated 1.4×10^9 ϕ decays in 2 years (2001–2002) with a maximum luminosity of up to $7.5 \times 10^{32}/\text{cm}^2/\text{s}$. KLOE resumed data taking in 2004 with an upgraded machine.

Production Experiments: Central Production and Two-Photon Fusion

In contrast to *formation* experiments like e^+e^- and $p\bar{p}$ annihilation discussed in the previous sections, the total energy in *production* experiments is shared among the recoiling particle(s) and the multi-meson final state. The mass and quantum numbers of the final state cannot be determined from the initial state and thus, many resonant waves with different angular momenta can contribute.

In central production, glueballs were suggested long time ago to be produced copiously

in the process [92]:

$$\text{hadron}_{\text{beam}} p \rightarrow \text{hadron}_f X p_s, \quad (17)$$

where the final-state hadrons carry large fractions of the initial-state hadron momenta and are scattered diffractively into the forward direction. To fulfill this requirement in a (proton) fixed-target experiment, a slow proton and a fast hadron needs to be observed in the final state. Mostly proton beams were used for these kinds of experiments, but some also involved pions or even kaons. The triggers in these experiments enhanced double-exchange processes – Reggeon-Reggeon, Reggeon-Pomeron, or Pomeron-Pomeron – relative to single-exchange and elastic processes. Early theoretical predictions suggested that the cross section for double-Pomeron exchange is constant with center-of-mass energy \sqrt{s} , whereas a falling cross section is expected for the other exchange mechanisms []:

$$\sigma (\text{Reggeon} - \text{Reggeon}) \sim 1/s \quad (18)$$

$$\sigma (\text{Reggeon} - \text{Pomeron}) \sim 1/\sqrt{s} \quad (19)$$

$$\sigma (\text{Pomeron} - \text{Pomeron}) \sim \text{constant} \quad (20)$$

At sufficiently high center-of-mass energies, reaction (17) is expected to be dominated by double-Pomeron exchange. The pomeron carries no charges – neither electric nor color charges – and is expected to have positive parity and charge conjugation. Thus, double-Pomeron exchange should favor production of isoscalar particles with positive G-parity in a glue-rich environment as no valence quarks are exchanged.

The observation in central production of a significant enhancement of glueball candidates over the production of conventional $q\bar{q}$ mesons at small transverse momenta led to the idea of a *glueball filter* [93]. No dynamical explanation has been given for this empirical finding, yet. In fact, the data show a strong kinematical dependence at small transverse momenta for all mesons. [Just a momentum filter?](#)

Several experiments, especially at CERN, made remarkable contributions. The WA76 Collaboration recorded data, mainly at 300 GeV/c, using a 60 cm long H₂ target. Multi-wire proportional chambers triggered on exactly one “fast” particle in the forward direction. Some results from WA76 can be found in [94].

The electromagnetic multiphoton spectrometer GAMS-2000 originally took data at the IHEP proton synchrotron, Protvino, in a 38 GeV/c negative-pion beam [95]. The detector was later upgraded for experiments at the CERN SPS [96]. GAMS-4000 used a 50 cm long liquid H₂ target and comprised a matrix of 64×64 lead glass cells covering almost 6 m².

Both the WA91 and WA102 Collaborations reported strong kinematical dependences of central meson production. The layout of the WA102 experiment is shown in Fig. 6. The experiment was a continuation of the WA76, WA91 and NA12/2 experiments at CERN aiming at a more complete study of the mass region from 1.2 to 2.5 GeV/c². The experimental setup was a combination of the WA76 setup serving as a charged-particle tracker and the GAMS-4000 detector in the forward region providing the opportunity to detect and study events with charged and neutral particles. Results from WA102 are summarized in [97–114].

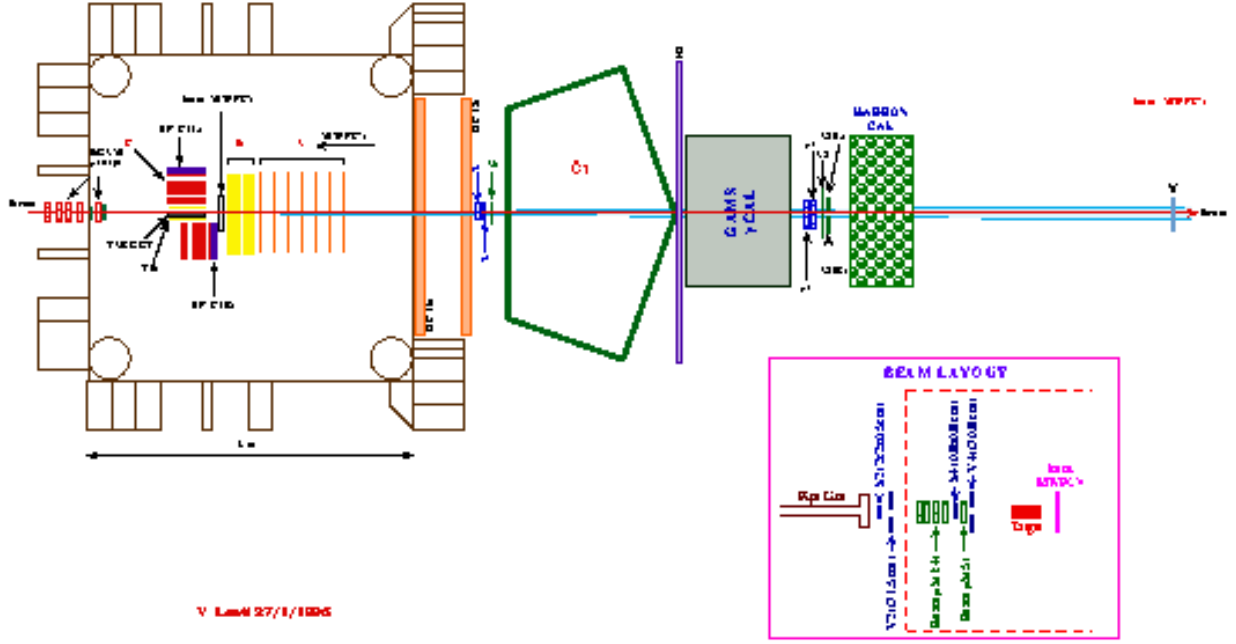


Figure 6: Layout of the WA102 experiment using the CERN Ω spectrometer and GAMS-4000 (1996 run) [Better picture?](#)

In contrast to direct glueball signals, the corresponding absence of states or glueball candidates in certain reactions can be as informative. Models predict for example that the $\gamma\gamma$ coupling of non- $q\bar{q}$ mesons is small and thus, glueball production should be suppressed in two-photon fusion. In addition to the *stickiness* (as defined in Eq. 13), a further quantitative test was proposed whether a meson state is a glueball or a conventional $q\bar{q}$ meson. In [17], the normalized quantity *gluiness* denotes the ratio of the two-gluon to the two-photon coupling of a particle and is expected to be near unity for a $q\bar{q}$ meson within the accuracy of the approximations made in [17]:

$$G = \frac{9e_Q^4}{2} \left(\frac{\alpha}{\alpha_s} \right)^2 \frac{\Gamma_{R \rightarrow gg}}{\Gamma_{R \rightarrow \gamma\gamma}} \quad (21)$$

Two-photon fusion has been studied in *production* with the CLEO II and upgraded CLEO II.V detectors at CESR using 13.3 fb^{-1} of e^+e^- data. The hadron is produced in the fusion of two space-like photons emitted by the beam electron and positron. Results of two-photon fusion studies from CLEO can be found in [90, 115].

Further results on the $\gamma\gamma$ -width of mesons have been reported by the LEP program at CERN. Though mainly focussing on electroweak physics, significant results on meson spectroscopy were achieved. The 4π detector ALEPH was designed to give as much detailed information as possible about complex events in high-energy e^+e^- collisions [116]. A su-

perconducting coil produced a uniform 1.5-T field in the beam direction. Inside the coil, in order of increasing radius, there was a microstrip solid-state device, an Inner Tracking Chamber (ITC) using drift wires, a 3.6×4.4 m Time Projection Chamber (TPC), and an electromagnetic calorimeter of 2 mm lead sheets with proportional wire sampling. A hadron calorimeter and a double layer of drift tubes aiding in good electron/muon identification were located outside the magnet coil. ALEPH data-taking ended on November 2000. The L3 detector was designed to measure the energy and position of leptons with the highest obtainable precision allowing a mass resolution of $\delta m/m$ smaller than 2% in dilepton final states [117]. Hadronic energy flux was detected by a fine-grained calorimeter, which also served as a muon filter and a tracking device. The outer boundary of the detector was given by the iron return-yoke of a conventional magnet. The field was 0.5 T over a length of 12 m. Radially inwards was a combined hadron calorimeter and muon absorber. The electromagnetic energy flow was determined by approximately 11,000 BGO crystals. Full electromagnetic shower containment over nearly 4π solid angle coverage was achieved. L3 data-taking ended on November 2000. Important ALEPH and L3 results on the $\gamma\gamma$ -width of mesons are given in [118–120].

Other Experiments

Many more experiments have significantly contributed to meson spectroscopy though these were not particularly devoted to the glueball search. Pion- and kaon beams were exploited in charge-exchange reactions:

$$\pi^-(K^-) + \text{proton} \rightarrow \text{neutron} + \text{meson} \quad (22)$$

In case of a kaon-induced reaction, the baryon in the final state can also be a Λ baryon.

The LASS facility at SLAC was developed for strangeonium spectroscopy [121]. This spectrometer was designed for charged-particle final states and based on a superconducting solenoid producing a 2.24 T field along the beam axis and a subsequent 3 Tm dipole magnet with a vertical field. Particles under large scattering angles at low momenta and high-energy secondaries could be detected, respectively, with very good angular and momentum resolution. The LASS Collaboration recorded over $135 \cdot 10^6$ kaon-induced events.

The VERTex Spectrometer (VES) setup at Protvino was a large-aperture magnetic spectrometer including systems of proportional and drift chambers, a multi-channel threshold Čerenkov counter, beam-line Čerenkov counters, a lead-glass γ -detector (LGD) and a trigger hodoscope. This arrangement permits full identification of multi-particle final states. A negative particle beam (π^- , K^-) with momenta between 20-40 GeV/ c was provided by the 70 GeV/ c proton synchrotron. A description of the setup can be found in [122].

Experiment E852 at the Brookhaven Alternating Gradient Synchrotron had a dedicated program to study mainly mesons with exotic quantum numbers. The experimental setup was based on the Multi-Particle Spectrometer (MPS) and used a 30-cm liquid hydrogen target. It was surrounded by a cylindrical drift chamber to track charged particles downstream of the target and an array of barrel-shaped thallium-doped CsI crystals, all located inside the MPS dipole magnet [123]. Photons were detected in a 3000-element lead glass detector (LGD)

Name	Mass [MeV/ c^2]	Width [MeV/ c^2]	Decays
$f_0(600)$	400 – 1200	600 – 1000	$\pi\pi, \gamma\gamma$
$f_0(980)$	980 ± 10	40 – 100	$\pi\pi, K\bar{K}, \gamma\gamma$
$f_0(1370)$	1200 – 1500	200 – 500	$\pi\pi, \rho\rho, \sigma\sigma, \pi(1300)\pi, a_1\pi, \eta\eta, K\bar{K}$
$f_0(1500)$	1505 ± 6	109 ± 7	$\pi\pi, \sigma\sigma, \rho\rho, \pi(1300)\pi, a_1\pi, \eta\eta, \eta\eta'$ $K\bar{K}, \gamma\gamma$
$f_0(1710)$	1724 ± 7	137 ± 8	$\pi\pi, K\bar{K}, \eta\eta, \omega\omega, \gamma\gamma$
$f_0(1790)$			
$f_0(2020)$	1992 ± 16	442 ± 60	$\rho\pi\pi, \pi\pi, \rho\rho, \omega\omega, \eta\eta$
$f_0(2100)$	2103 ± 8	209 ± 19	$\eta\pi\pi, \pi\pi, \pi\pi\pi\pi, \eta\eta, \eta\eta'$
$f_0(2220)$	2189 ± 13	238 ± 50	$\pi\pi, K\bar{K}, \eta\eta$
$f_0(2330)$	2314 ± 25	200	$\pi\pi, \eta\eta$

Table 6: The $I = 0$, $J^{PC} = 0^{++}$ mesons as listed by the particle data group [7].

matching the downstream aperture of the MPS magnet [124]. All reactions were induced by a 18 GeV/ c π^- beam.

Heavy-Flavor Experiments

4.2 The scalar, pseudoscalar and tensor mesons

If we focus on the expected three lightest mass glueballs, $J^{PC} = 0^{++}$, 2^{++} , and 0^{-+} , we note that these are all quantum numbers of normal $q\bar{q}$ mesons. As such, it is important to understand what the known spectra and multiplet assignments of these states are. As a starting point, we take the point of view of the particle data group (PDG) [7]. The $I = 0$ mesons are listed for $J^{PC} = 0^{++}$ in Table 6, $J^{PC} = 2^{++}$ in Table 7 and $J^{PC} = 0^{-+}$ in Table 8. The following sections describe the main experimental findings in the search for the lightest-mass glueballs.

Results from $p\bar{p}$ Annihilation: The Crystal Barrel Experiment

The Crystal Barrel experiment [1] studied $p\bar{p}$ annihilation both at rest and in flight and observed final states with multiple charged particles and photons. In particular, many all-neutral final states were observed for the first time. The experiment accumulated about 10^8 $p\bar{p}$ annihilation at rest in liquid hydrogen and thus, exceeded statistics collected in bubble-chamber experiments by about three orders of magnitude. At the beginning of the Crystal-Barrel data taking in late 1989, only three scalar states were well established: $a_0(980)$, $f_0(980)$, and the $K_0^*(1430)$. The high-statistics data sets collected at rest provided firm evidence for new states, among others the $f_0(1500)$ scalar state.

Name	Mass [MeV/c ²]	Width [MeV/c ²]	Decays
$f_2(1270)$	1275.1 ± 1.2	$185^{+2.9}_{-2.4}$	$\pi\pi, \pi\pi\pi\pi, K\bar{K}, \eta\eta, \gamma\gamma$
$f_2(1430)$	1430	13 – 150	$K\bar{K}, \pi\pi$
$f'_2(1525)$	1525 ± 5	73^{+6}_{-5}	$K\bar{K}, \eta\eta, \pi\pi, K\bar{K}^* + cc$
$f_2(1565)$	1565 ± 13	134 ± 8	$\pi\pi, \rho\rho, \eta\eta, a_2\pi, \omega\omega, K\bar{K}, \gamma\gamma$
$f_2(1640)$	1639 ± 6	99^{+60}_{-40}	$\omega\omega, 4\pi, K\bar{K}$
$f_2(1810)$	1815 ± 12	197 ± 22	$\pi\pi, \eta\eta, 4\pi, K\bar{K}$
$f_2(1910)$	1903 ± 9	140 – 200	$\pi\pi, K\bar{K}, \eta\eta, \omega\omega, \eta'\eta', \eta'\eta', \rho\rho$
$f_2(1950)$	1944 ± 12	472 ± 18	$K^*\bar{K}^*, \pi\pi, 4\pi, a_2\pi, f_2\pi\pi, \eta\eta, K\bar{K}, \gamma\gamma$
$f_2(2010)$	2011^{+62}_{-76}	202^{+67}_{-62}	$\phi\phi, K\bar{K}$
$f_2(2150)$	2156 ± 11	167 ± 30	$\pi\pi, \eta\eta, K\bar{K}, f_2\eta, a_2\pi$
$f_2(2300)$	2297 ± 28	149 ± 41	$\phi\phi, K\bar{K}, \gamma\gamma$
$f_2(2340)$	2339 ± 55	319^{+81}_{-69}	$\phi\phi, \eta\eta$

Table 7: The $I = 0, J^{PC} = 2^{++}$ mesons as listed by the particle data group [7].

Name	Mass [MeV/c ²]	Width [MeV/c ²]	Decays
$\eta(548)$	547.51 ± 0.018	$1.30 \pm .07$ keV	$\gamma\gamma, 3\pi$
$\eta'(958)$	957.78 ± 0.14	0.203 ± 0.016	$\eta\pi\pi, \rho\gamma, \omega\gamma, \gamma\gamma$
$\eta(1295)$	1294 ± 4	55 ± 5	$\eta\pi\pi, a_0\pi, \gamma\gamma, \eta\sigma, K\bar{K}\pi$
$\eta(1405)$	1409.8 ± 2.5	51.3 ± 34	$K\bar{K}\pi, \eta\pi\pi, a_0\pi, f_0\eta, 4\pi$
$\eta(1475)$	1476 ± 4	87 ± 9	$K\bar{K}\pi, K\bar{K}^* + cc, a_0\pi, \gamma\gamma$
$\eta(1760)$	1756 ± 9	96 ± 70	$\omega\omega, 4\pi$
$\eta(2225)$	2220 ± 18	150^{+300}_{-60}	$K\bar{K}K\bar{K}$

Table 8: The $I = 0, J^{PC} = 0^{-+}$ mesons as listed by the particle data group [7].

Crystal Barrel studied proton-antiproton annihilations at rest into three pseudoscalar mesons: $p\bar{p} \rightarrow \pi^0\pi^0\pi^0$ [53, 54], $p\bar{p} \rightarrow \pi^0\pi^0\eta$ [53], $p\bar{p} \rightarrow \pi^0\eta\eta$ [53, 55, 56], $p\bar{p} \rightarrow \pi^0\eta\eta'$ [57], $p\bar{p} \rightarrow K_L^0 K_S^0 \pi^0$ [58], $p\bar{p} \rightarrow K_L^0 K_S^0 \eta$ [58], $p\bar{p} \rightarrow K^+ K^- \pi^0$ [59], $p\bar{p} \rightarrow K_L K_L \pi^0$ [60], $p\bar{p} \rightarrow \pi^0\pi^0\eta'$ [61], $p\bar{p} \rightarrow \eta\pi\pi$ [62], $n\bar{p} \rightarrow \pi^-\pi^0\pi^0$ [68], $n\bar{p} \rightarrow \pi^+\pi^-\pi^-$ [69], into four pseudoscalar mesons: $p\bar{p} \rightarrow \eta\pi^0\pi^0\pi^0$ [63], and into five pions: $p\bar{p} \rightarrow 5\pi$ [64–67]. In addition, the reactions $p\bar{p} \rightarrow \omega\pi^0\pi^0$ [70], $n\bar{p} \rightarrow \omega\pi^-\pi^0$ [71], were analyzed.

There were also measurements made in flight at several different incident \bar{p} momenta: $p\bar{p} \rightarrow K\bar{K}\pi^0$ [72], $p\bar{p} \rightarrow \eta\pi^0\pi^0$ [73], $p\bar{p} \rightarrow \eta\pi^0\pi^0\pi^0$ [74], $p\bar{p} \rightarrow \omega\pi^0$ [75], $p\bar{p} \rightarrow \omega\eta$ [75], $p\bar{p} \rightarrow \omega\eta'$ [75], $p\bar{p} \rightarrow \pi^0\pi^0\pi^0$ [76], $p\bar{p} \rightarrow \pi^0\pi^0\eta$ [76], $p\bar{p} \rightarrow \pi^0\eta\eta$ [76], $p\bar{p} \rightarrow K^+ K^- \pi^0$ [76].

The first experimental hint for an isoscalar state around 1500 MeV/c² came in 1973 from a low-statistics analysis of $p\bar{p}$ annihilations at rest into three pions [125]. The state was later

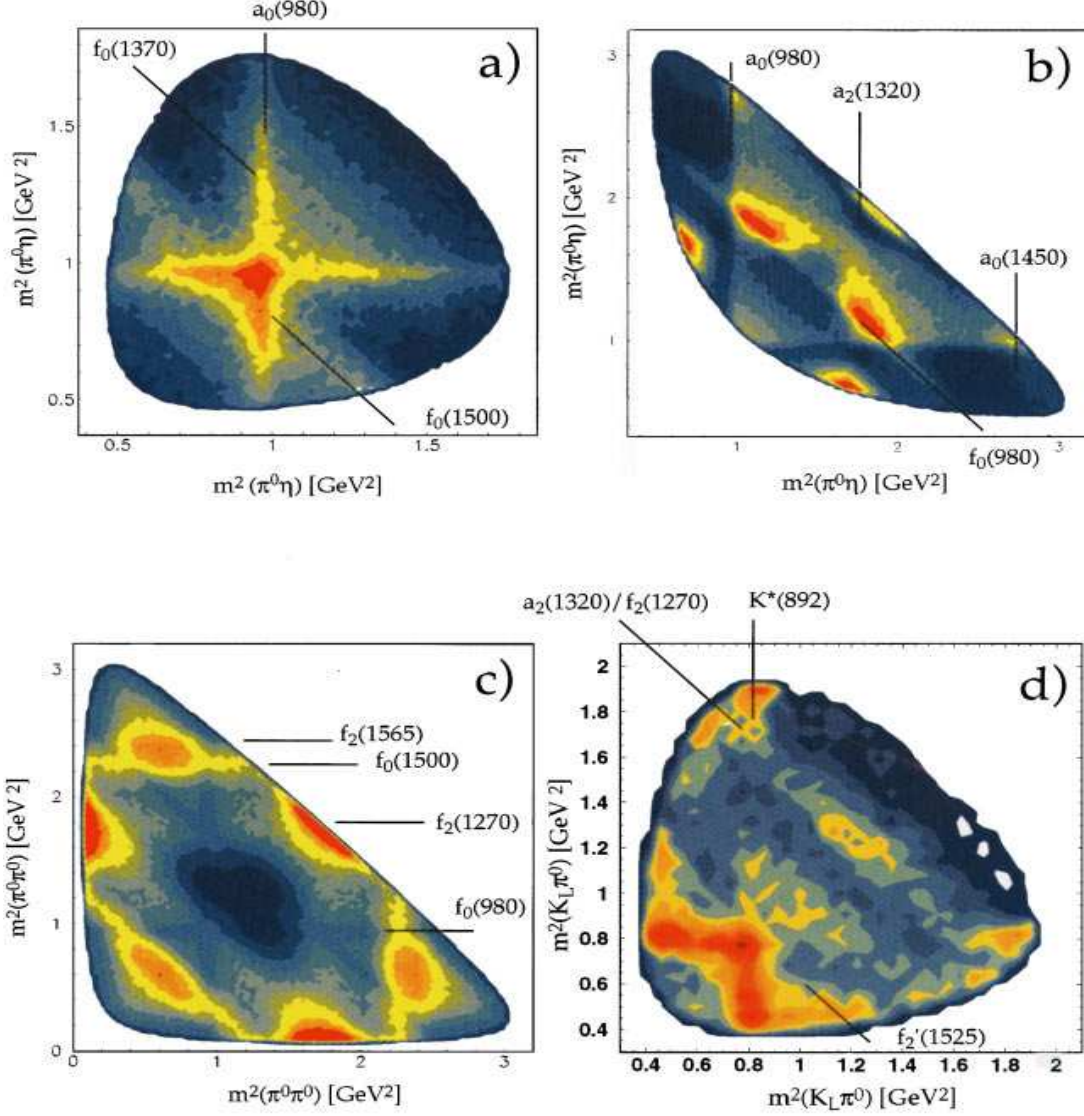


Figure 7: Dalitz plots for $p\bar{p}$ annihilation at rest from Crystal Barrel into (a) $\pi^0 \eta \eta$ ($\sim 2 \times 10^5$ events), (b) $\pi^0 \pi^0 \eta$ ($\sim 2.8 \times 10^5$ events), (c) $3\pi^0$ ($\sim 700,000$ events), (d) $\pi^0 K_L K_L$ ($\sim 37,000$ events). All events are entered more than once for symmetry reasons. Figure taken from [2].

confirmed with a mass of $1527 \text{ MeV}/c^2$ suggesting a spin-0 assignment and also reporting a missing $K\bar{K}$ decay mode [126]. A very broad, somewhat higher-mass S-wave state called $G(1590)$ was reported in $38 \text{ GeV}/c$ pion-induced reactions by the GAMS-2000 Collaboration decaying to $\eta\eta$ [127] and $\eta\eta'$ [128]. The group reported that the decay rate into two neutral pions is at least three times lower than the rate into $\eta\eta$.

Crystal Barrel provided high-statistics for final states with three light pseudoscalar mesons. In summary, a consistent description of all these data was achieved in a coupled-channel anal-

ysis by using four (isoscalar) scalar $\pi^0\pi^0$ waves: $f_0(980)$, $f_0(1370)$, $f_0(1500)$, and a broad structure $f_0(400 - 1200)$ – listed as $f_0(600)$ by the PDG. In particular, the $3\pi^0$ and $\pi^0\eta\eta$ channels need the two scalar states, $f_0(1370)$ and $f_0(1500)$, decaying to $\pi^0\pi^0$ and $\eta\eta$. Consistency in the description of the data sets further requires two poles for the $\eta\pi^0$ S-wave in annihilation into $\pi^0\pi^0\eta$, $a_0(980)$ and $a_0(1450)$, in addition to a tensor meson in the $\pi\pi$ P-wave, $f_2(1565)$ [53].

Dalitz plots from various Crystal Barrel analyses are shown in Fig. 7 for $p\bar{p}$ annihilation into $\pi^0\eta\eta$ (a), $\pi^0\pi^0\eta$ (b), $3\pi^0$ (c), and $\pi^0 K_L K_L$ (d). The most prominent features are labeled in the figure. The Dalitz plot for proton-antiproton annihilation into $\pi^0\eta\eta$ is dominated by the crossing vertical and horizontal bands for the isovector state $a_0(980)$ decaying into $\pi\eta$ (Fig. 7 (a)). The data also demand two isoscalar states, labeled $f_0(1370)$ and $f_0(1500)$, decaying to $\eta\eta \rightarrow 6\gamma$ [56]. In fact, an earlier analysis based on a reduced $\pi^0\eta\eta$ data set provided the first evidence for the $f_0(1370)$ [55]. The observation of two necessary scalar states decaying to $\eta\eta$ is confirmed in an analysis of the $\pi^0\eta\eta \rightarrow 10\gamma$ final state, which exhibits entirely different systematics. It is now widely accepted that the $f_0(1500)$ observed by Crystal Barrel in the coupled-channel analysis with a K-matrix mass and width of $M \sim 1569 \text{ MeV}/c^2$ and $\Gamma \sim 191 \text{ MeV}/c^2$ is identical to the $G(1590)$ observed by the GAMS Collaboration [127].

A narrow band of about constant intensity is observed in the $3\pi^0$ Dalitz plot (Fig. 7 (c)) indicating the presence of the $f_0(1500)$. Further visible features include an increased population at the edges of the Dalitz plot along the $\pi\pi$ band marked $f_2(1270)$. This indicates that one decay π^0 is preferentially emitted along the flight direction of the resonance, which is typical of a spin-2 resonance decaying with an angular distribution of $(3\cos^2\theta - 1)^2$ from the 1S_0 initial state. Striking are the corner blobs, which follow a $\sin^2\theta$ angular distribution and correspond to the $f'_2(1525)$ interfering constructively with the two $\pi\pi$ S-waves. The fit also requires a small contribution from the $f_2(1565)$.

An important piece of information to clarify the internal structure of the $f_0(1500)$ is to study its $K\bar{K}$ decay mode. In fact, no strange decay was reported by a previous bubble-chamber experiment [126], which had very limited statistics and no partial wave analysis was performed. The Dalitz plot for the $\pi^0 K_L K_L$ channel at rest from Crystal Barrel is shown in Fig. 7 (d). One K_L was missing in the analysis and the other K_L interacted hadronically in the CsI calorimeter. Events with three clusters in the barrel were used for the analysis [60]. The contributions from the $f_0(1370)$ and $f_0(1500)$ were found to be small. The precise determination is however challenging because the isovector state $a_0(1450)$ also decays to $K_L K_L$, which can form both an $I = 0$ and $I = 1$ system. Contributions from $a_0(1450)$ were thus determined from the $K_L K^\pm \pi^\mp$ final state by using isospin conservation and the fact that no isoscalar S-wave contributes.

The 4π decay modes of scalar mesons were studied at rest in proton-antiproton annihilation into $5\pi^0$ [65] and $3\pi^0\pi^+\pi^-$ [64] as well as in antiproton-neutron annihilation into $4\pi^0\pi^-$ [66,67] and $2\pi^0 2\pi^-\pi^+$ [67]. All data sets are dominated by 4π scalar isoscalar interactions and at least the two states, $f_0(1370)$ and $f_0(1500)$, are required in the analysis. It is observed that the 4π -decay width of the $f_0(1370)$ is more than 6 times larger than the sum of all observed partial decay widths to two pseudoscalar mesons. This may indicate a

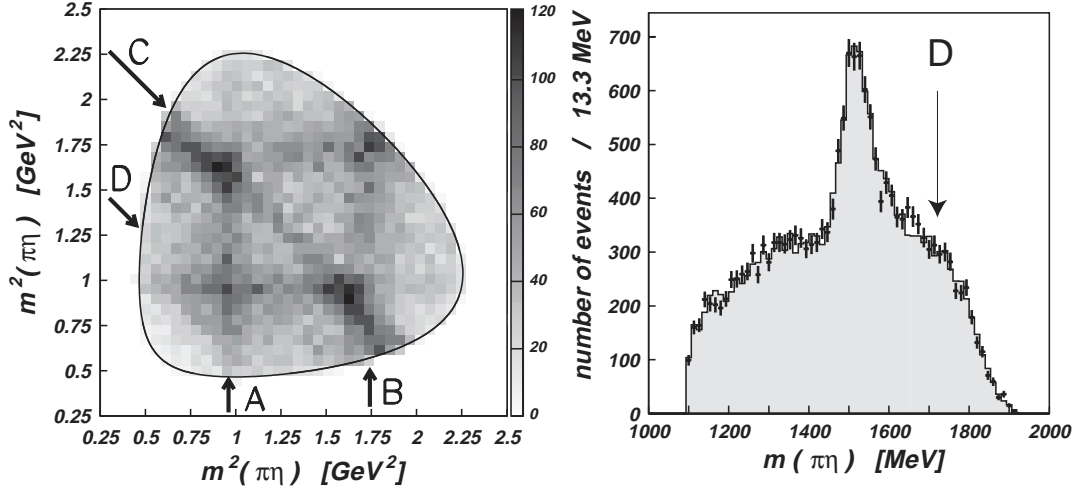


Figure 8: Dalitz plot for $p\bar{p} \rightarrow \pi^0\eta\eta$ in flight at 900 MeV/c (left). The arrows indicate $a_0(980)$ (A), $a_2(1320)$ (B), $f_0(1500)/f'_2(1525)$ (C), whereas (D) shows the expected location of the $f_0(1710)$. The $\eta\eta$ mass projection (right) is dominated by the $f_0(1500)/f'_2(1525)$ peak; the shaded area represents the fit [76]. Figure taken from [5].

dominant $n\bar{n}$ component over a $s\bar{s}$ structure. The 4π -decays of the $f_0(1500)$ represent about half of its total width. The analyses also yield important couplings to $(\pi\pi)_S(\pi\pi)_S$ and to $\rho\rho$ (Table 9). It was pointed out in [129] that the $\rho\rho$ decay should dominate $2[\pi\pi]_S$ if the $f_0(1500)$ was a mixture of the ground state glueball with nearby $q\bar{q}$ states, at least in the framework of the 3P_0 $Q\bar{Q}$ pair creation model. In leading order of this scheme, the decay mechanism of the $f_0(1500)$ proceeds dominantly via its quarkonia components. Unfortunately, results from Crystal Barrel and WA102 entirely disagree leaving the experimental situation unsettled (Tables 9 and 10).

In the limit of no s -quark admixture in the proton wave function, the OZI rule does not support production of pure $s\bar{s}$ states in $p\bar{p}$ annihilation. For this reason, observation of the $f_0(1710)$ scalar state should be strongly suppressed, which is assumed to have a dominant $s\bar{s}$ component. The state was discovered by the Crystal-Ball Collaboration in radiative J/ψ decays into $\eta\eta$ [131], but the spin ($J = 0$ or 2) remained controversial for a long time. The WA102 Collaboration later determined the spin in favor of 0^{++} in central production at 450 GeV/c. Crystal Barrel data for the reactions $p\bar{p} \rightarrow \pi^0\pi^0\pi^0$, $p\bar{p} \rightarrow \pi^0\pi^0\eta$, and $p\bar{p} \rightarrow \pi^0\eta\eta$ in flight at 900 MeV/c were used to search for isoscalar 0^{++} and 2^{++} states in the 1000-2000 MeV/c² mass range, in particular for the $f_0(1710)$ [76]. A satisfactory signal around 1700 MeV/c² was neither observed for a scalar nor for a tensor state in the partial wave analyses of both the $\pi^0\pi^0\pi^0$ and $\pi^0\eta\eta$ channels. The $\pi^0\eta\eta$ Dalitz plot and the corresponding $\eta\eta$ mass projection are shown in Fig. 8. The (D) arrow indicates the expected location of the $f_0(1710)$. None of the fits using the PDG mass and width for the $f_0(1710)$ had a stable solution and the log-likelihood improvement was not significant even in the best fit. The

Ratio	$f_0(1370)$	$f_0(1500)$
$\Gamma(K\bar{K}) / \Gamma(\pi\pi)$	$(0.37 \pm 0.16) \text{ to } (0.98 \pm 0.42)$ [67]	^a 0.186 ± 0.066 [54, 60] ^b 0.119 ± 0.032 [53]
$\Gamma(\eta\eta) / \Gamma(\pi\pi)$	0.020 ± 0.010 [67]	^a 0.226 ± 0.095 [54, 56] ^b 0.157 ± 0.062 [53]
$\Gamma(\eta\eta') / \Gamma(\pi\pi)$		^a 0.066 ± 0.028 [54, 57] ^b 0.042 ± 0.015 [53]
$\Gamma(\rho\rho) / \Gamma(4\pi)$	0.260 ± 0.070 [66]	0.130 ± 0.080 [66, 67]
$\Gamma(\sigma\sigma) / \Gamma(4\pi)$	0.510 ± 0.090 [66]	0.260 ± 0.070 [66]
$\Gamma(\rho\rho) / \Gamma(2[\pi\pi]_S)$		0.500 ± 0.340 [66]
$\Gamma(4\pi) / \Gamma_{\text{tot}}$	0.800 ± 0.050 [130]	0.760 ± 0.080 [66]

Table 9: A summary of Crystal-Barrel results on the decay of scalar mesons. Branching ratios for decays into 4π are determined from $\bar{p}n$ annihilation. Results labeled ^a are from single channel analyses and ^b from a coupled channel analysis including $3\pi^0$, $2\pi^0\eta$, and $\pi^0\eta\eta$.

state does not seem to be produced in proton-antiproton annihilations in flight at 900 MeV/ c and upper limits at the 90 % confidence level were derived using PDG mass and width of $M = 1715 \text{ MeV}/c^2$ and $\Gamma = 125 \text{ MeV}/c^2$ [132]:

$$\frac{\mathcal{B}(p\bar{p} \rightarrow \pi^0 f_0(1710) \rightarrow \pi^0 \pi^0 \pi^0)}{\mathcal{B}(p\bar{p} \rightarrow \pi^0 f_0(1500) \rightarrow \pi^0 \pi^0 \pi^0)} < 0.31 \quad (23)$$

$$\frac{\mathcal{B}(p\bar{p} \rightarrow \pi^0 f_0(1710) \rightarrow \pi^0 \eta\eta)}{\mathcal{B}(p\bar{p} \rightarrow \pi^0 f_0(1500) \rightarrow \pi^0 \eta\eta)} < 0.25 \quad (24)$$

For this reason, the non-observation of the $f_0(1710)$ scalar state in $p\bar{p}$ reactions is consistent with a dominant $s\bar{s}$ assignment to this state assuming it has a $q\bar{q}$ structure. Though the WA102 Collaboration supported this conclusion by reporting a much stronger $K\bar{K}$ coupling of the $f_0(1710)$ than $\pi\pi$ coupling, it was not directly observed in the amplitude analysis of the reaction $K^-p \rightarrow K_S K_S \Lambda$. As mentioned before, the spin assignment was controversial for a long time and much later settled in favor of 0^{++} . In fact, the assumption in the analysis of K^- -induced data was $J = 2$ and may explain the absence.

[Results on pseudoscalar states ...](#)

Results from the OBELIX Experiment

The OBELIX detector system was operated at LEAR with a liquid H_2 (D_2) target, a gaseous H_2 target at room temperature and pressure, and a target at low pressures (down to 30 mbar). Among other things, the wide range of target densities provided detailed information about the influence of the atomic cascade on the annihilation process.

The collaboration has performed several studies looking at the $\eta(1405)$ and $\eta(1460)$ in the $K\bar{K}\pi$ final states. The first study looked at $p\bar{p} \rightarrow K^\pm K_{miss}^0 \pi^\mp \pi^+ \pi^-$ at rest [47] where they confirmed two pseudoscalar states. The lighter decayed mainly to $K\bar{K}\pi$ (via $a_0(980)\pi$) while the heavier to K^*K . Further evidence for the two states is provided in references [48] and [49]. A study of the reaction $\pi_1(1400)$ from $p\bar{p} \rightarrow K^+ K^- \pi^+ \pi^- \pi^0$ [50] at rest in a gaseous hydrogen target provides information on the $\eta(1405)$ and $\eta(1460)$. Also hints of the $f_0(1710)$ decaying to $f_0(1370)(\pi\pi)_S$ were found.

OBELIX also observed an isovector scalar state with a mass of about 1.3 GeV/ c^2 in its $K\bar{K}$ decay mode [51, 52]; the state is relatively narrow, with a 80 MeV width. In formation, the collaboration reported on the 3π decays of the $\pi(1300)$ as well as suggested a 3π decay of the $\pi_1(1400)$ from $p\bar{p} \rightarrow 2\pi^+ 2\pi^-$ [46] at rest and in flight.

The OBELIX Collaboration recently studied the $\pi^+ \pi^- \pi^0$, $K^+ K^- \pi^0$, and $K^\pm K^0 \pi^\mp$ final states in proton-antiproton annihilation at rest at three different hydrogen target densities in the framework of a coupled-channel analysis together with $\pi\pi$, πK , and $K\bar{K}$ scattering data [52]. One of the main goals of the analysis was to determine branching ratios as well as $\pi\pi$ and $K\bar{K}$ partial widths of all the involved ($J^P = 0^+, 1^-, 2^+$) resonances. Dalitz-plot projections of the three annihilation reaction are shown in Fig. 9. The scattering data, in particular the $\theta_0(\pi\pi \rightarrow \pi\pi)$ phase shift, clearly require contributions from the $f_0(980)$ pole. The authors further report on two additional poles required by annihilation data, a broad $f_0(1370)$ and a relatively narrow $f_0(1500)$. The introduction of a fourth scalar state improves the data and splits the initially broad $f_0(1370)$ into a broad $f_0(400 - 1200)$ and a relatively narrow $f_0(1370)$. The $f_0(1710)$ does not seem to be needed by the data. In addition, a good description requires the $f_2(1270)$ and $f'_2(1525)$ tensor states. The $f_2(1565)$ pole is needed for the $\pi^+ \pi^- \pi^0$ and $K^+ K^- \pi^0$ data at low pressure and in hydrogen gas at normal temperature and pressure. The following $\Gamma_{K\bar{K}}/\Gamma_{\pi\pi}$ ratios of branching fractions for $f_0(1370)$, $f_0(1500)$, and $f_2(1270)$ were determined:

$$\frac{\mathcal{B}(p\bar{p} \rightarrow f_0(1370)\pi^0, f_0 \rightarrow K\bar{K})}{\mathcal{B}(p\bar{p} \rightarrow f_0(1370)\pi^0, f_0 \rightarrow \pi\pi)} = \begin{cases} 1.000 \pm 0.200 & {}^1S_0 \\ 0.940 \pm 0.200 & {}^3P_1 \end{cases} \quad (25)$$

$$\frac{\mathcal{B}(p\bar{p} \rightarrow f_0(1500)\pi^0, f_0 \rightarrow K\bar{K})}{\mathcal{B}(p\bar{p} \rightarrow f_0(1500)\pi^0, f_0 \rightarrow \pi\pi)} = \begin{cases} 0.240 \pm 0.040 & {}^1S_0 \\ 0.300 \pm 0.040 & {}^3P_1 \end{cases} \quad (26)$$

$$\frac{\mathcal{B}(p\bar{p} \rightarrow f_2(1270)\pi^0, f_2 \rightarrow K\bar{K})}{\mathcal{B}(p\bar{p} \rightarrow f_2(1270)\pi^0, f_2 \rightarrow \pi\pi)} = \begin{cases} 0.043 \pm 0.010 & {}^1S_0 \\ 0.045 \pm 0.010 & {}^3P_1 \\ 0.048 \pm 0.010 & {}^3P_2 \end{cases} \quad (27)$$

The values for $f_0(1500)$ from OBELIX obtained in a coupled-channel framework are somewhat greater than earlier coupled-channel results from Crystal-Barrel (Table 9) and agree well with results from WA102 [104] (Table 10). The $f_2(1270)$ ratios agree with the PDG values within the experimental errors.

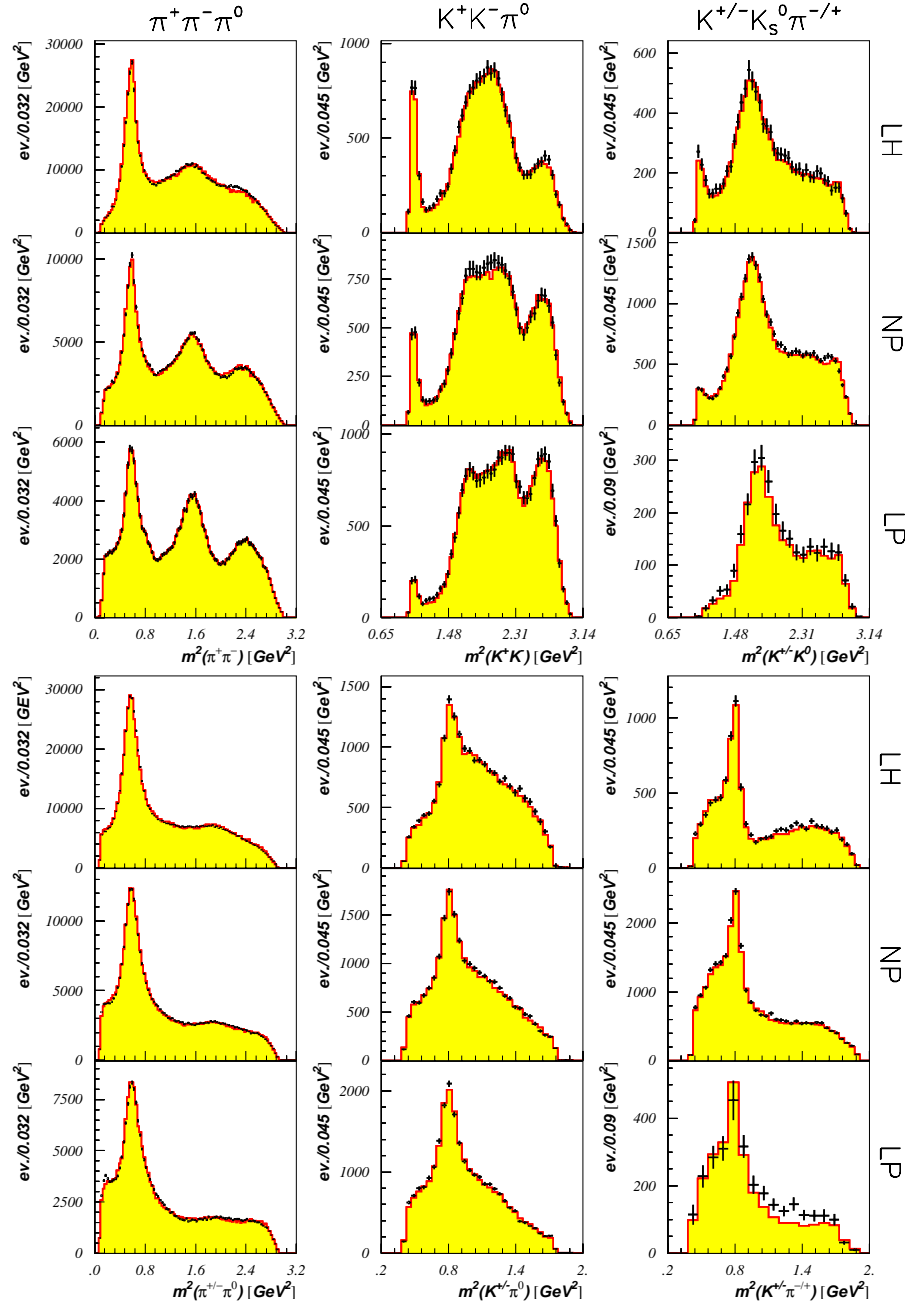


Figure 9: Theoretical (shaded histograms) and experimental (background subtracted) Dalitz-plot projections from the OBELIX experiment of the three annihilation reactions $p\bar{p} \rightarrow \pi^+\pi^-\pi^0$, $p\bar{p} \rightarrow K^+K^-\pi^0$, and $p\bar{p} \rightarrow K^\pm K_S^0 \pi^\mp$ in liquid (LH) hydrogen, H_2 gas at normal pressure and temperature (NP), and low pressure (LP) hydrogen gas. Theoretical and experimental errors are summed. Figure is taken from [52].

Scalar	$\pi\pi/K\bar{K}$	$\pi\pi/\eta\eta$	$\eta\eta/K\bar{K}$	$\rho\rho/2[\pi\pi]_S$	$\rho\rho/4\pi$	$\sigma\sigma/4\pi$
$f_0(1370)$	2.17 ± 0.90		0.35 ± 0.21		~ 0.9	~ 0
$f_0(1500)$	3.13 ± 0.68	5.5 ± 0.84		2.6 ± 0.4^1 3.3 ± 0.5^2	0.74 ± 0.03	0.26 ± 0.03
$f_0(1710)$	0.20 ± 0.03		0.48 ± 0.14			

Table 10: A summary of WA102 results on the decay of scalar mesons [97–103, 105, 114]. The result for the decay of the $f_0(1500)$ into 4π is derived ¹ from $2\pi^+2\pi^-$ and ² from $\pi^+\pi^-2\pi^0$.

Results from Central Production: The WA102 Experiment

The WA102 experiment looked at 450 GeV/c protons incident on a proton target to study the reaction $pp \rightarrow p_{(f)ast} X p_{(s)low}$ – so-called *central production*. Such reactions are believed to have a significant contribution from double-pomeron exchange – a reaction that is supposed to be glue-rich. Relevant to the search for scalar glueballs, the collaboration carried out partial wave analysis on a large number of final states. $pp \rightarrow pp4\pi$ [97–100], $pp \rightarrow pp\pi^0\pi^0$ [101], $pp \rightarrow pp\pi^+\pi^-$ [97, 102, 104], $pp \rightarrow ppK^+K^-$ [103, 104], $pp \rightarrow ppK_S^0K_S^0$ [103], $pp \rightarrow pp\eta\eta$ [106], $pp \rightarrow pp\eta\eta'$ [105], $pp \rightarrow pp\eta'\eta'$ [105], $pp \rightarrow pp\eta\eta$ [106], $pp \rightarrow pp\phi\phi$ [107], $pp \rightarrow pp\omega\omega$ [108], $pp \rightarrow pp\phi\omega$ [109] and $pp \rightarrow ppK^*(892)\bar{K}^*(892)$ [109].

In addition, a number of studies that bear on the search from pseudoscalar states were also performed: $pp \rightarrow pp\pi^0\pi^0\pi^0$ [110], $pp \rightarrow pp\pi^+\pi^-\pi^0$ [111], $pp \rightarrow pp\eta\pi^0$ [112], $pp \rightarrow pp\eta\pi^+\pi^-$ [113], and $pp \rightarrow ppK\bar{K}\pi$ [114].

Results of measured decay branching ratios into two pseudoscalar mesons are listed in Table 10 [97–103, 105, 114]. Further selected PWA results from the WA102 experiment on central production are presented in Fig. 10 [6, 104–106]. The K^+K^- S-wave from a coupled-channel analysis of $\pi^+\pi^-$ and K^+K^- data is shown in (a). The long tail beyond the dominant threshold enhancement for the $f_0(980)$ includes signals for the three scalar resonances of Table 10. Only the two higher-mass states are observed as peaks [104]. The corresponding K^+K^- D-wave (b) shows resonant peaks for the two established tensor mesons $f_2(1270)$ and $f_2'(1525)$. A structure at 2.15 GeV/ c^2 is also observed in the mass distribution. The pole positions for the $f_0(1370)$ and $f_0(1500)$ are in excellent agreement with results from the Crystal-Barrel experiment. Fig. 10 (c) and (d) present the $\eta\eta$ S- and D-wave [106]. The $f_0(1500)$ is clearly seen in the S-wave $\eta\eta$ mass distribution (c). In addition to a weak $f_2(1270)$ signal, the resonant structure at 2.15 GeV/ c^2 is also observed in the $\eta\eta$ D-wave (d). The $f_0(1500)$ was also observed in studies of the $\eta\eta'$ decay mode [105], shown in Fig. 10 (e), and in the 4π final state [99].

The small $\Gamma(\pi\pi)/\Gamma(K\bar{K})$ value for the $f_0(1710)$ in Table 10 clearly indicates that this resonance must have a large $s\bar{s}$ component. By contrast, the same ratio is much greater than one for the $f_0(1500)$. If interpreted as $q\bar{q}$ state, the $f_0(1500)$ cannot have a large $s\bar{s}$ component since pure $s\bar{s}$ mesons do not decay to pions. Moreover, we recall that an enhancement of gluonic states is expected in Pomeron-Pomeron fusion (Close-Kirk glueball filter) [93]. Though the $f_0(1710)$ couples more strongly to $K\bar{K}$, the K^+K^- S-wave signal

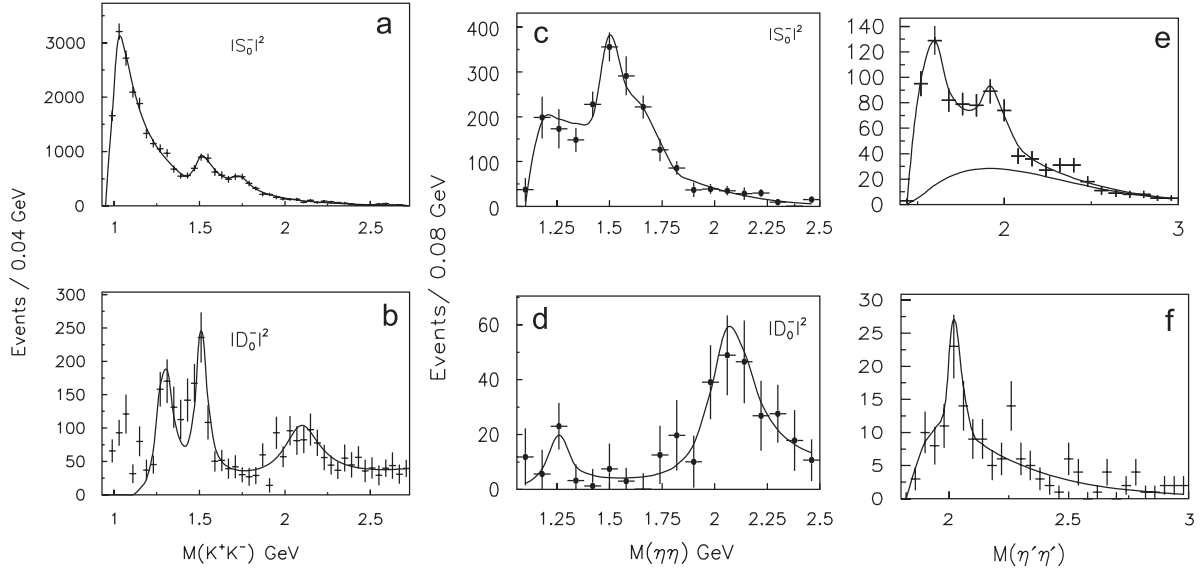


Figure 10: K^+K^- S- (a) and D-wave (b) from a coupled-channel analysis of WA102 $\pi^+\pi^-$ and K^+K^- data [104]. The T-matrix formalism was used for overlapping resonances to account for unitarity. Signals for $f_0(1500)$ and $f_0(1710)$ are clearly observed. Mass distributions for $\eta\eta$ S- and D-wave are shown in (c) and (d). The right panel shows $\eta\eta'$ (e) and $\eta'\eta'$ (f) mass distributions.

for the $f_0(1500)$ shown in Fig. 10 (a) is larger in agreement with predictions of the glueball filter. [Comment on the \$\rho\rho/2\[\pi\pi\]_S\$ disagreement with CB](#)

Table 11 shows further results on resonance production from WA102. The cross section is given at 450 GeV/c for the reaction

$$pp \rightarrow p_f X p_s,$$

and the dependence of the production of X on the parameter dP_T , denoting the difference in transverse momentum between the particles exchanged from the fast and slow vertices. Production of $X = \rho^0$ with $I = 1$ cannot proceed via double-Pomeron exchange (DPE). The $\pi^+\pi^-$ mass spectra from the WA76 Collaboration at $\sqrt{s} = 12.7$ GeV and $\sqrt{s} = 23.8$ GeV [94] show a reduction of the ρ^0 yield at higher center-of-mass energies. The Collaboration reports a cross section ratio of 0.44 ± 0.07 indicating that DPE becomes more important with increasing energy.

Table 11 also shows that production of isovector states is strong, e.g. the $a_1(1260)$, which requires Reggeon exchange.

Scalar resonances are consistent with Pomeron-Pomeron fusion. Production of $a_0(980)$ is suppressed by almost a factor of 10 with respect to the $f_0(980)$. The $a_0(1450)$ is not even seen, whereas a large $f_0(1500)$ yield is observed. Interestingly, production of the $f_0(1710)$ is very weak.

J^{PC}	Res.	σ [nb]	$dP_T \leq 0.2$ GeV	$0.2 \leq dP_T \leq 0.5$ GeV	$dP_T \geq 0.5$ GeV
0^{-+}	π^0	$22\,011 \pm 3\,267$	12 ± 2	45 ± 2	43 ± 2
	η	$3\,859 \pm 368$	6 ± 2	34 ± 2	60 ± 3
	η'	$1\,717 \pm 184$	3 ± 2	32 ± 2	64 ± 3
0^{++}	$a_0(980)$	638 ± 60	25 ± 4	33 ± 5	42 ± 6
	$f_0(980)$	$5\,711 \pm 450$	23 ± 2	51 ± 3	26 ± 3
	$f_0(1370)$	$1\,753 \pm 580$	18 ± 4	32 ± 2	50 ± 3
	$f_0(1500)$	$2\,914 \pm 301$	24 ± 2	54 ± 3	22 ± 4
	$f_0(1710)$	245 ± 65	26 ± 2	46 ± 2	28 ± 2
	$f_0(2000)$	$3\,139 \pm 480$	12 ± 2	38 ± 3	50 ± 4
1^{++}	$a_1(1260)$	$10\,011 \pm 900$	13 ± 3	51 ± 4	36 ± 3
	$f_1(1285)$	$6\,857 \pm 1\,306$	3 ± 1	35 ± 2	61 ± 4
	$f_1(1420)$	$1\,080 \pm 385$	2 ± 2	38 ± 2	60 ± 4
2^{++}	$a_2(1320)$	$1\,684 \pm 134$	10 ± 2	38 ± 5	52 ± 6
	$f_2(1270)$	$3\,275 \pm 422$	8 ± 1	29 ± 1	63 ± 2
	$f'_2(1520)$	68 ± 9	4 ± 3	36 ± 3	60 ± 4
	$f_2(1910)$	528 ± 40	20 ± 4	62 ± 7	18 ± 4
	$f_2(1950)$	$2\,788 \pm 175$	27 ± 2	46 ± 5	27 ± 2
	$f_2(2150)$	121 ± 12	3 ± 3	53 ± 4	44 ± 3

Table 11: A summary of WA102 results on resonance production at $\sqrt{s} = 29.1$ GeV [133]. The quoted errors are statistical and systematic errors summed in quadrature. Numbers given for resonance production as a function of dP_T are percentages of the total contribution.

Though, scalar meson production indicates dominant (glue-rich) Pomeron-Pomeron exchange, the situation for other resonances is less clear. [Elaborate more on validity of double-pomeron exchange](#)

Light Mesons from e^+e^- Experiments: The BES Experiment

Several reactions have been studied in the BES experiment. Partial wave analysis has been performed on several radiative decays of the J/ψ and are reported for the following reactions: $J/\psi \rightarrow \gamma\pi^+\pi^-\pi^+\pi^-$ [80], $J/\psi \rightarrow \gamma\pi^+\pi^-$ [81], $J/\psi \rightarrow \gamma\pi^0\pi^0$ [81], $J/\psi \rightarrow \gamma K^+K^-$ [82], $J/\psi \rightarrow \gamma K_S^0 K_S^0$ [82], and $J/\psi \rightarrow \gamma\phi\omega$ [83]. In addition to the radiative decays, BES has also examined decays to associated vector meson decays. Here, analysis has been performed on the reactions: $J/\psi \rightarrow \omega\pi^+\pi^-$ [84], $J/\psi \rightarrow \phi\pi^+\pi^-$ [85], $J/\psi \rightarrow \omega K^+K^-$ [86], and $J/\psi \rightarrow \phi K^+K^-$ [85].

BES II results on J/ψ radiative decays to $\pi^+\pi^-$ and $\pi^0\pi^0$ are shown in Fig. 11. A sample of 58 M J/ψ events was used for the PWA [81]. Similar structures are visible in both mass spectra. Three clear peaks are observed in both distributions in the 1.0 to 2.3 GeV/ c^2 mass

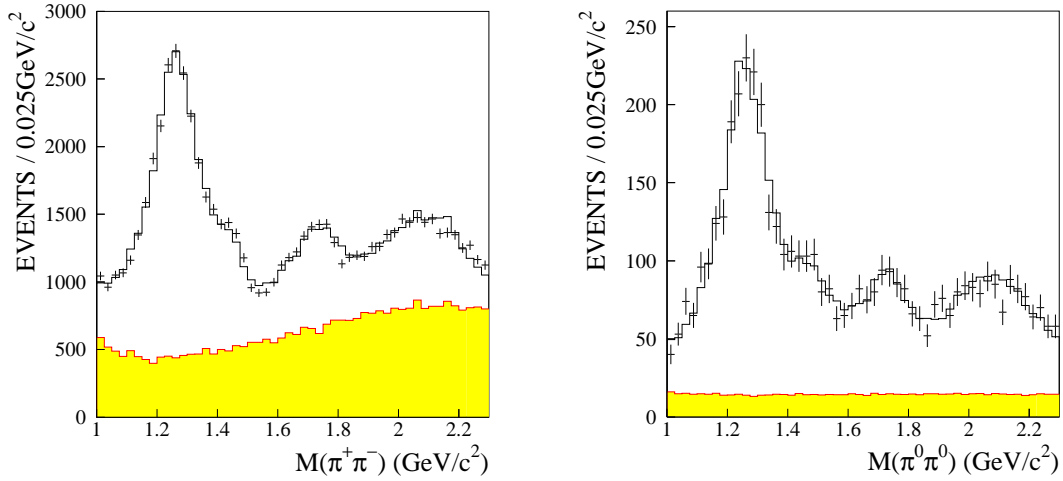


Figure 11: The $\pi^+\pi^-$ invariant mass distribution (a) and the $\pi^0\pi^0$ mass distribution (b) from the reaction $J/\psi \rightarrow \gamma\pi\pi$ from BES [81]. The crosses are data, the full histogram shows the maximum likelihood fit, and the shaded area corresponds to the background.

range: a strong $f_2(1270)$ signal exhibiting a shoulder on the high-mass side, an enhancement at $\sim 1.7 \text{ GeV}/c^2$ associated with the $f_0(1710)$, and a peak at $\sim 2.1 \text{ GeV}/c^2$. The shaded histogram in Fig. 11 (a) corresponds to dominant background from $J/\psi \rightarrow \pi^+\pi^-\pi^0$. The estimated background in (b) stems from various reactions; PDG branching ratios have been used in the studies. Three scalar mesons are observed with approximately consistent results from both fits. The lowest 0^{++} state is consistent with the $f_0(1500)$ and associated with the shoulder in Fig. 11. The collaboration reports that spin 0 is strongly preferred over spin 2 in the analysis. Though not favored in the PWA, the presence of the $f_0(1370)$ is not excluded. The fitted masses and widths from $J/\psi \rightarrow \gamma\pi^+\pi^-$ for the two lowest-mass states are given by:

$$\begin{aligned} M_{f_0(1500)} &= 1466 \pm 6 \pm 20 \text{ MeV}/c^2 & \Gamma &= 108_{-11}^{+14} \pm 25 \text{ MeV}/c^2 \\ M_{f_0(1710)} &= 1765_{-3}^{+4} \pm 13 \text{ MeV}/c^2 & \Gamma &= 145 \pm 8 \pm 69 \text{ MeV}/c^2, \end{aligned}$$

whereas PDG values for the $f_0(2020)$ are used for the structure at $\sim 2.1 \text{ GeV}/c^2$.

The two established scalar mesons, $f_0(1500)$ and $f_0(1710)$, are also significantly produced in $J/\psi \rightarrow 2\pi^+ 2\pi^-$ with masses of $M_{f_0(1500)} = 1505_{-20}^{+15}$ and $M_{f_0(1710)} = 1740_{-25}^{+30}$, respectively [80]. In addition, the likelihood fit requires a tensor state $f_2(1950)$ around $2 \text{ GeV}/c^2$ confirming earlier WA91 and WA102 results [98, 134]. Branching fractions determined from $J/\psi \rightarrow 2\pi^+ 2\pi^-$ are listed in Table 12. The $f_0(1710)$ scalar state also dominates the reaction $J/\psi \rightarrow \gamma K \bar{K}$. Evidence for the $f_0(1500) \rightarrow K \bar{K}$ is however insignificant, but included in the partial wave analysis interfering with the $f_0(1710)$. For a description of the $1500 \text{ MeV}/c^2$ mass range, the $f'_2(1525)$ tensor state is required in the analysis [82].

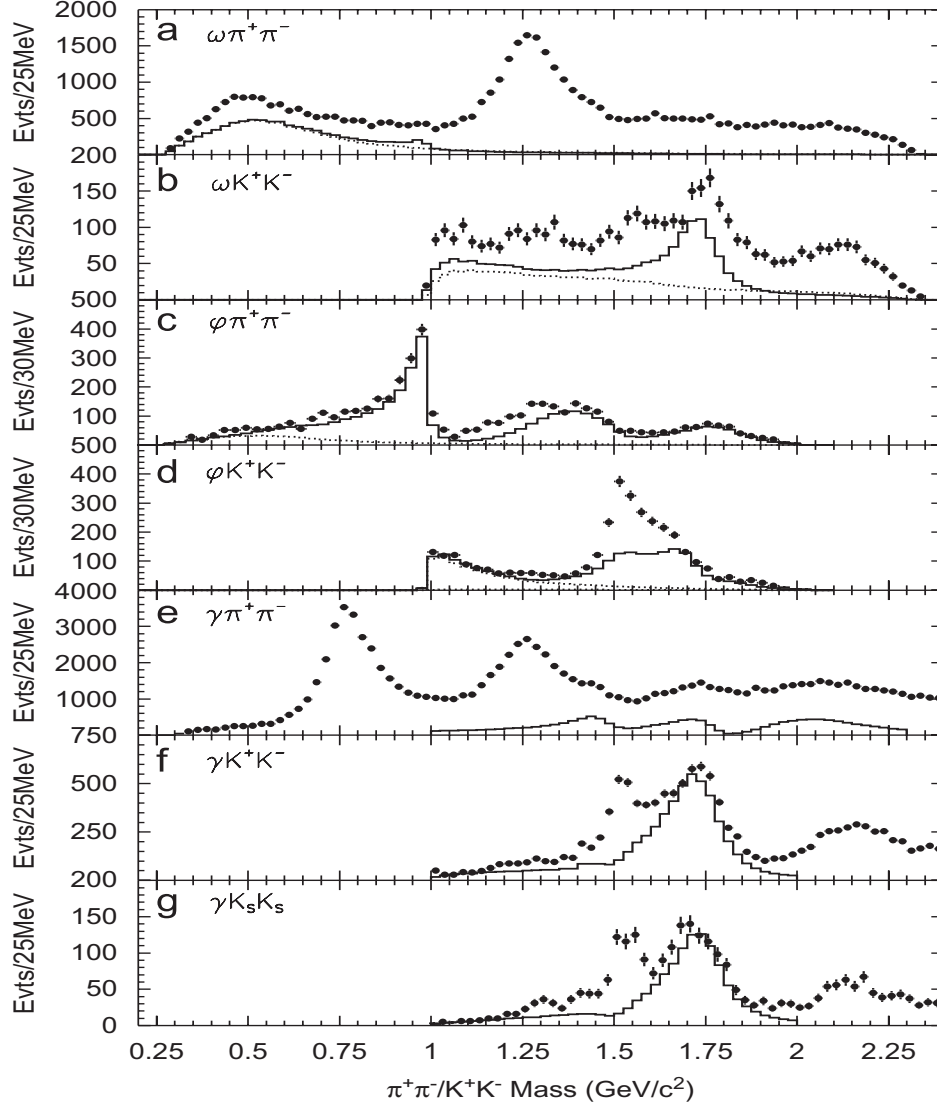


Figure 12: Invariant mass distributions of pseudoscalar meson pairs recoiling against ω , ϕ or γ in J/ψ decays measured at BES II. The dots with error bars are data, the solid histograms are the scalar contributions from PWA, and the dashed lines in (a) through (c) are contributions of $\sigma(485)$ from the fits, while the dashed line in (d) is the $f_0(980)$. Notice that not the full mass spectra are analyzed in (e), (f), and (g). The figure is taken from [135].

In section 4.1, we have discussed the *flavor-tagging* approach to study the flavor content of mesons in J/ψ decays. Due to the OZI rule, $J/\psi \rightarrow \omega X$ couples to the $n\bar{n}$ component of X , while $J/\psi \rightarrow \phi X$ couples to $s\bar{s}$. Fig. 12 shows invariant mass distributions of pseudoscalar meson pairs recoiling against ω , ϕ or γ [135]. The K^+K^- mass distribution from ωK^+K^- (b) shows a clear scalar peak at 1710 MeV/ c^2 which is not observed in the corresponding spectrum recoiling against the ϕ meson (d). By contrast, the $\pi^+\pi^-$ mass distribution from

Scalar	$\pi^+\pi^-$ [81]	$\pi^0\pi^0$ [81]	$K\bar{K}$ [82]	$\pi^+\pi^-\pi^+\pi^-$ [80]
$f_0(1500)$	0.67 ± 0.30	0.34 ± 0.15		3.1 ± 1.12
$f_0(1710)$	2.64 ± 0.75	1.33 ± 0.88	$9.62 \pm 0.29_{\text{stat}}$	3.1 ± 1.12
$f_0(2100)$				5.1 ± 1.82
$f_2(1270)$	9.14 ± 1.48	4.00 ± 0.59		1.8 ± 0.63
$f_2'(1525)$			$3.42 \pm 0.15_{\text{stat}}$	
$f_2(1565)$				3.2 ± 1.12
$f_2(1950)$				5.5 ± 1.92

Table 12: BES results on radiative J/ψ decays. The rates are shown for $J/\psi \rightarrow \gamma f_0$ with the subsequent decay of the f_0 to the listed final state. All rates are multiplied by 10^{-4} . The quoted errors are statistical and systematic errors summed in quadrature.

$\phi\pi^+\pi^-$ (c) indicates an enhancement at $\sim 1790 \text{ MeV}/c^2$, which is absent in ϕK^+K^- (d). This observation is puzzling and does not seem to be compatible with a single $f_0(1710)$ state, which is known to decay dominantly to $K\bar{K}$. The BES collaboration suggested two distinct scalar states around $1.75 \text{ GeV}/c^2$: the known $f_0(1710)$ with ($M \sim 1740 \text{ MeV}/c^2$, $\Gamma \sim 150 \text{ MeV}/c^2$) decaying strongly to $K\bar{K}$ and a broad $f_0(1790)$ with ($M \sim 1790 \text{ MeV}/c^2$, $\Gamma \sim 270 \text{ MeV}/c^2$) which couples more strongly to $\pi\pi$ [85]. This new state is not confirmed by any other experiment and not listed in the 2008 edition of the “Review of Particle Physics” by the Particle Data Group [136]. The BES collaboration emphasizes that the $\phi f_0(1790)$ signal is very close to edge of the available phase space, where the reconstruction efficiency of the ϕ decreases significantly as the momentum of the ϕ decreases. Tails of broad higher-mass states could also interfere with the $f_0(1710)$ generating a structure near the end of the phase space [135]. If both states really exist, it remains a mystery why the $f_0(1710)$ mainly $s\bar{s}$ -state is produced recoiling against an ω , and the new $f_0(1790)$ mainly $n\bar{n}$ -state is observed recoiling against a ϕ . In fact, it’s worth noting that many strong signals due to non-strange states are seen in the $\phi\pi\pi$ data from BES: $f_2(1270)$, $f_0(1370)$, $f_0(1500)$, and $f_0(1790)$. The collaboration makes a strong argument for the existence of a $f_0(1370)$ resonance, which has been doubted previously by several authors. In the analysis, the state interferes with the $f_0(1500)$ and $f_2(1270)$ making it more noticeable, but a determination of its mass and width is challenging for the same reason.

A recent BES observation has increased the scalar puzzle even more. The group observes a state at $M \sim 1812 \text{ MeV}/c^2$ and $\Gamma \sim 105 \text{ MeV}/c^2$ in the doubly OZI suppressed process $J/\psi \rightarrow \gamma\omega\phi$ [83]. The PWA favors a 0^+ scalar assignment. The state is listed as $X(1835)$ by the PDG, but has not been seen by another experiment. The production ratio should be suppressed by at least an order of magnitude. A value of $\mathcal{B}(J/\psi \rightarrow \gamma X) \cdot \mathcal{B}(X \rightarrow \omega\phi) = (2.61 \pm 0.27 \text{ (stat)} \pm 0.65 \text{ (syst)}) \times 10^{-4}$ is reported. Decay rates for the discussed mesons are listed in Table 12. Moreover, BES reports the ratios of branching fractions into $\pi\pi$ and

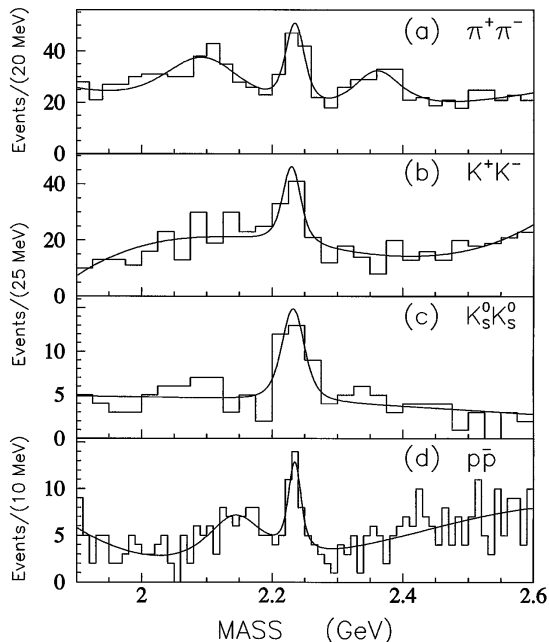


Figure 13: Fitted invariant mass spectra of a) $\pi^+\pi^-$, b) K^+K^- , c) $K_S^0K_S^0$, and d) $p\bar{p}$ from BES suggesting the existence of the $f_J(2220)$. An unbinned maximum-likelihood method was applied using a smooth background plus one or several Breit-Wigners resonances convoluted with Gaussian resolution functions [137].

$K\bar{K}$ for the $f_0(1370)$ [85] and $f_0(1710)$ [86]:

$$\frac{\mathcal{B}(f_0(1370) \rightarrow K\bar{K})}{\mathcal{B}(f_0(1370) \rightarrow \pi\pi)} = 0.08 \pm 0.08 \quad (28)$$

$$\frac{\mathcal{B}(f_0(1710) \rightarrow \pi\pi)}{\mathcal{B}(f_0(1710) \rightarrow K\bar{K})} < 0.11 \text{ (@ 95 \% C.L.)} \quad (29)$$

Evidence for the 2^{++} and 0^{-+} glueballs are weak. The BES Collaboration observed signals in radiative J/ψ decays for the $f_J(2220)$, also known as $\xi(2230)$, in a sample of more than 5×10^6 J/ψ decays in final states including $K\bar{K}$, $\pi^+\pi^-$, and $p\bar{p}$ [137, 138]. Fig. 13 shows the fitted invariant mass spectra. The signal was first observed by the MARK-III Collaboration and published in 1985 in the reactions $J/\psi \rightarrow \gamma K_S^0 K_S^0$ and $J/\psi \rightarrow \gamma K^+ K^-$ based on a sample of 5.8×10^6 J/ψ decays [139]. However, limits on the product branching fraction, $\mathcal{B}(J/\psi \rightarrow \gamma f_J(2220)) \cdot \mathcal{B}(f_J(2220) \rightarrow K^+ K^-)$, reported by the DM2 Collaboration were in disagreement with the MARK-III findings [140]. The first indication for a spin-2 particle came from the GAMS Collaboration in 1986. They observed a signal at $2220 \text{ MeV}/c^2$ decaying to $\eta\eta'$ in the $\eta\eta'n$ final state from pion-induced reaction on the proton [141]. This finding was in agreement with the original result from radiative J/ψ decays. Many other experiments carefully searched for the $f_J(2220)$ in proton-antiproton annihilation in-flight, but no evidence was found of this state [142–147]. A high-statistics search in 2000 by the Crystal-Barrel Collaboration also showed no narrow state [148]. If the state really exists, it has a very large branching fraction in radiative J/ψ decays. Future experimental efforts with the BES-III detector may shed some light on the possible existence of this state.

Light Mesons from the CLEO Experiment

Radiative $\Upsilon(1S)$ decays also provide a glue-rich environment for producing exotic states. The CLEO Collaboration has reported on results from $\Upsilon(1S)$ decays to pairs of pseudoscalar mesons [77, 78]. Considering the fact that the quark-photon coupling is proportional to the electric charge and assuming that the quark propagator is roughly proportional to $1/m$ for low-momentum quarks, radiative decays from $\Upsilon(1S)$ should be suppressed by a factor of

$$(q_b/q_c)^2 \cdot (m_c/m_b)^2 \cdot \Gamma_\Upsilon/\Gamma_\psi \approx 0.04 \quad (30)$$

relative to the corresponding J/ψ decay. Table 13 summarizes the results. In particular, the decay rates of $f_0(1500)$ and $f_0(1710)$ to $\pi^0\pi^0$ are much smaller – by more than an order of magnitude – than predicted based on the scalar-glueball mixing matrix in [37].

The two listed tensor states dominate the di-gluon spectrum in $\Upsilon(1S)$ decays and fair agreement with the naive scaling argument is observed (to the same order of magnitude) for the suppression factor of these states relative to J/ψ decays.

Scalar	$\Upsilon(1S) \rightarrow \gamma + \text{meson}$	$\pi^+\pi^-$	$\pi^0\pi^0$	K^+K^-	$\pi^+\pi^-\pi^+\pi^-$	$\eta\eta$
$f_0(980)$	< 1.5	< 3				
$f_0(1500)$		< 1.5				< 0.3
$f_0(1710)$			< 0.14	< 0.7		< 0.18
$f_2(1270)$	10.2 ± 0.8 [77]	3.0 ± 0.5				
$f'_2(1525)$	$3.7^{+0.9}_{-0.7}$ [77]					

Table 13: CLEO results on radiative $\Upsilon(1S)$ decays. The rates for the scalar mesons are upper-limit branching fractions at the 90 % confidence level for $\Upsilon \rightarrow \gamma f_0$ with the subsequent decay of the f_0 to the listed final state. All rates are multiplied by 10^{-5} .

Three-body decays of D -mesons may provide a test of the microscopic structure of scalar mesons. CLEO published the results of Dalitz-plot analyses for $D^0 \rightarrow \pi^+\pi^-\pi^0$ and $D^+ \rightarrow \pi^+\pi^+\pi^-$ [88, 89]. They observe a highly-suppressed $f_0(980)$ meson in the reaction $D^0 \rightarrow f_0(980)\pi^0$. Though the suppression itself is in good agreement with predictions inserting rescattering effects and considering the $f_0(980)$ as $s\bar{s}$ + a light $q\bar{q}$ pair [149], the calculated ratio $\mathcal{B}(D^+ \rightarrow f_0(980)\pi^+)/\mathcal{B}(D^0 \rightarrow f_0(980)\pi^0)$ of 46.7 is almost an order of magnitude smaller than the experimentally determined lower limit of > 340 @ 95 % confidence level.

[Further results on \$D\$ decays from Belle, BaBar, etc.](#)

Further Results from Photon-Photon Fusion

Apart from proving the existence of particular states, crucial to establishing the glueball nature of any glueball candidate is an anti-search in two-photon collisions since gluonic states do not couple directly to photons. Results from $\gamma\gamma$ collisions were reported by the LEP collaborations. Fig. 14 (left side) shows three peaks below 2 GeV in the invariant

$K_S^0 K_S^0$ mass distribution observed by the L3 collaboration [118]. The background is fitted by a second-order polynomial and the three peaks by Breit-Wigner functions. The mass spectrum is dominated by the formation of tensor mesons, the $f_2'(1525)$ and the $f_2(1270)$ interfering with the $a_2^0(1320)$. A clear signal for the $f_J(1710)$ is observed and found to be dominated by the spin-two helicity-two state. No resonance is observed in the $2.2 \text{ GeV}/c^2$ mass region. The $f_0(1500)$ scalar meson is not seen in its decay to $K_S^0 K_S^0$ in agreement with central-production data indicating a small $s\bar{s}$ component if this state is interpreted as $q\bar{q}$ meson. Fig. 14 (right side) shows the fitted $\pi^+\pi^-$ spectrum measured by the ALEPH collaboration in $\gamma\gamma$ collisions. Only the $f_2(1270)$ is observed and no signals for the $f_0(1500)$ and $f_J(1710)$. Upper limits for the decay into $\pi^+\pi^-$ have been determined at the 95 % confidence level:

$$\Gamma(\gamma\gamma \rightarrow f_0(1500)) \cdot \mathcal{B}(f_0(1500) \rightarrow \pi^+\pi^-) < 0.31 \text{ keV} \quad (31)$$

$$\Gamma(\gamma\gamma \rightarrow f_J(1710)) \cdot \mathcal{B}(f_J(1710) \rightarrow \pi^+\pi^-) < 0.55 \text{ keV} \quad (32)$$

The CLEO collaboration has reported on the possible glueball candidate $f_J(2220)$. An upper limit of $\Gamma_{\gamma\gamma} \mathcal{B}(f_J(2220) \rightarrow K_S^0 K_S^0) \leq 1.1$ eV at 95 % C.L. was derived from two-photon interactions, $\gamma\gamma \rightarrow f_J \rightarrow K_S^0 K_S^0$, using the CLEO II detector [90]. The same approach for the $f_2'(1525)$ leads to consistent results with PDG values. The CLEO observation is in agreement with the published result from the L3 Collaboration (Fig. 14) of $\Gamma_{\gamma\gamma} \mathcal{B}(f_J \rightarrow K_S^0 K_S^0) \leq 1.4$ eV at 95 % C.L. [118]. The non-observation of a signal in the $2.2 \text{ GeV}/c^2$ mass region in two-photon fusion is certainly expected for a true glueball, but the non-existence of this narrow state is also not excluded. The CLEO authors determine a large lower limit for the “stickiness” of > 109 at the 95 % C.L.

Two pseudoscalar mesons are reported in the $1400\text{-}1500 \text{ MeV}/c^2$ mass region and have been listed as two separate states by the Particle Data Group since ?, the $\eta(1405)$ and $\eta(1475)$. Long time considered only one resonance, the $\eta(1475)$ was first observed in two-photon collisions in 2001 decaying to $K\bar{K}\pi$ by the L3 Collaboration [119]. The reported two-photon partial width is 212 ± 50 (stat.) ± 23 (sys.) eV. The second η state is neither observed in $K\bar{K}\pi$ nor in $\eta\pi\pi$ by L3, suggesting a large gluonic content of the $\eta(1405)$. In 2005, CLEO published the non-observation of any pseudoscalar meson below $1700 \text{ MeV}/c^2$ based on 5 times more statistics with an upper limit of $\Gamma_{\gamma\gamma}(1440) \mathcal{B}(K\bar{K}\pi) < 89$ eV in disagreement with the L3 results. Only two-ground state axial vector mesons were reported in this mass range consistent with quark model expectations [115].

5 Gluonic Excitations

5.1 *Mixing in the scalar sector*

There have been many authors who have considered that the $f_0(1370)$, the $f_0(1500)$ and the $f_0(1710)$ are the physical manifestations of the underlying 0^{++} quarkonium nonet and the lowest mass glueball. It is generally assumed that the three bare states mix to yield the three physical states. Inputs to such calculations include the masses of the physical states

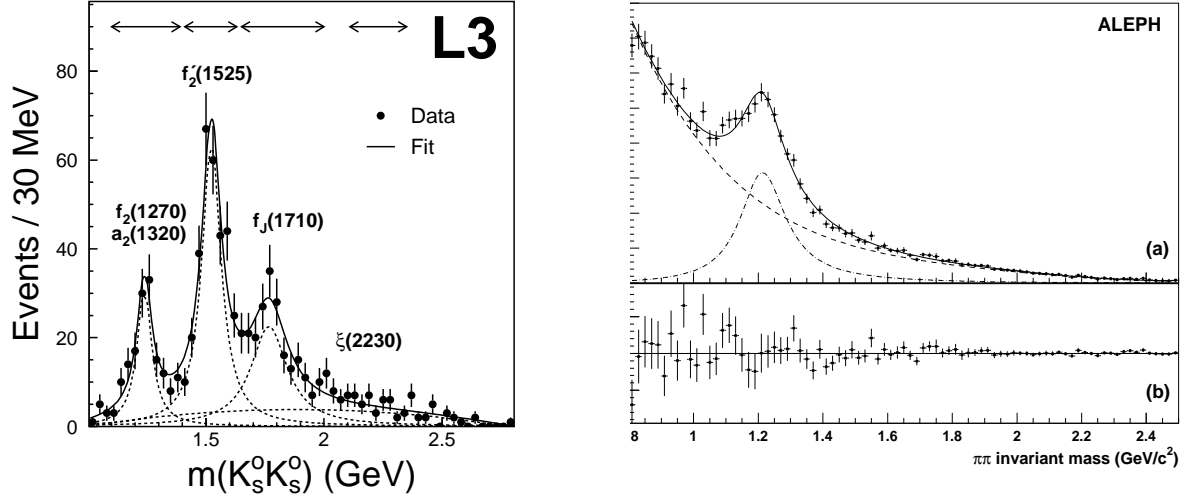


Figure 14: Left: invariant $K_S^0 K_S^0$ mass in $\gamma\gamma$ collisions from L3. The solid line corresponds to a maximum-likelihood fit. The arrows represent the $f_2(1270) - a_2^0(1320)$, the $f_2'(1525)$, the $f_J(1710)$, and the $\xi(2230)$ mass regions [118]. Right: invariant $\pi^+ \pi^-$ mass distribution from ALEPH. The top plot (a) shows the fit to the data using a Breit-Wigner function for the $f_2(1270)$ (dot-dashed line), a polynomial for the background (dashed line) and the combination of these functions (solid line). The bottom plot (b) shows the data after subtraction of the fitted curves. Only statistical error bars are shown [120].

as well as their decay rates into pairs of pseudoscalar mesons. The masses of the bare states and the mixing of the physical states then result. In addition to the choice of physical states, there appears to also be some dependence on whether one assumes the bare glueball is more or less massive than the mostly $s\bar{s}$ state.

In the literature, the mixing is typically written in terms of equation 33, where the physical states, $f_{1,2,3}$ are identified with the $f_0(1370)$, $f_0(1500)$ and $f_0(1710)$ respectively, and the bare states are parametrized in terms of the ideally mixed $q\bar{q}$ states:

$$\begin{aligned} n\bar{n} &= \frac{1}{\sqrt{2}} (u\bar{u} + d\bar{d}) \\ s\bar{s} & \end{aligned}$$

. However, it is also useful to look at these in terms of the SU(3) symmetric states as well

$$\begin{aligned} |1\rangle &= \frac{1}{\sqrt{3}} (u\bar{u} + d\bar{d} + s\bar{s}) \\ |1\rangle &= \frac{1}{\sqrt{6}} (u\bar{u} + d\bar{d} - 2s\bar{s}) \end{aligned}$$

$$\begin{pmatrix} |f_1\rangle \\ |f_2\rangle \\ |f_3\rangle \end{pmatrix} = \begin{pmatrix} M_{1n} & M_{1s} & M_{1g} \\ M_{2n} & M_{2s} & M_{2g} \\ M_{3n} & M_{3s} & M_{3g} \end{pmatrix} \cdot \begin{pmatrix} |n\bar{n}\rangle \\ |s\bar{s}\rangle \\ |G\rangle \end{pmatrix} \quad (33)$$

There is also some model dependence included in the analysis.

Broadly speaking, the results divide into two categories. The first in which the bare glueball comes out lighter than the $s\bar{s}$ state, and the second in which the bare glueball comes out heavier than the $s\bar{s}$ state. We summarize these by first looking at the case where the bare glueball is lighter. One of the earliest of these came from Close and Amsler [9,10]. They allowed for the rate of $s\bar{s}$ quark production from the vacuum to be different from the u and d quarks. They also allowed for the bare glueball to have a different coupling to $s\bar{s}$ than from $u\bar{u}$ and $d\bar{d}$. However, in their work, the resulting couplings were generally consistent with the flavor-blind assumption. Based mostly on results from the CrysTal Barrel experiment, they found a mixing as given in equation 34.

$$\begin{aligned}
\begin{aligned}
|f_0(1370)\rangle & \\
|f_0(1500)\rangle & \\
|f_0(1710)\rangle &
\end{aligned}
&= \begin{pmatrix} -0.91 & -0.07 & 0.40 \\ -0.41 & 0.35 & -0.84 \\ 0.09 & 0.93 & 0.36 \end{pmatrix} \cdot \begin{aligned}
|n\bar{n}\rangle & \\
|s\bar{s}\rangle & \\
|G\rangle &
\end{aligned} \\
\begin{aligned}
|f_0(1370)\rangle & \\
|f_0(1500)\rangle & \\
|f_0(1710)\rangle &
\end{aligned}
&= \begin{pmatrix} -0.78 & -0.47 & 0.40 \\ -0.13 & -0.52 & -0.84 \\ 0.61 & -0.71 & 0.36 \end{pmatrix} \cdot \begin{aligned}
|1\rangle & \\
|8\rangle & \\
|G\rangle &
\end{aligned}
\end{aligned} \tag{34}$$

Close and colleagues [17] later extended this by including additional data and found a mixing scheme as given in equation 35.

$$\begin{aligned}
\begin{aligned}
|f_0(1370)\rangle & \\
|f_0(1500)\rangle & \\
|f_0(1710)\rangle &
\end{aligned}
&= \begin{pmatrix} 0.86 & 0.13 & -0.50 \\ 0.43 & -0.61 & -0.61 \\ 0.22 & 0.76 & 0.60 \end{pmatrix} \cdot \begin{aligned}
|n\bar{n}\rangle & \\
|s\bar{s}\rangle & \\
|G\rangle &
\end{aligned} \\
\begin{aligned}
|f_0(1370)\rangle & \\
|f_0(1500)\rangle & \\
|f_0(1710)\rangle &
\end{aligned}
&= \begin{pmatrix} 0.78 & 0.39 & -0.50 \\ 0.00 & 0.75 & 0.61 \\ 0.62 & -0.49 & 0.60 \end{pmatrix} \cdot \begin{aligned}
|1\rangle & \\
|8\rangle & \\
|G\rangle &
\end{aligned}
\end{aligned} \tag{35}$$

Giacosa [150] looked at mixing in an effective chiral approach. They took the couplings to be flavor blind, and carried out their analysis both with and without a direct decay of the glueball. In the case without direct decay, the decays proceed via the $q\bar{q}$ content of the states. For the case of the mass of the bare glueball lighter than the $s\bar{s}$ state, they found the solution in equation 36 for the case without a direct glueball decay and that in equation 37 for the case with a direct glueball decay.

$$\begin{aligned}
\begin{aligned}
|f_0(1370)\rangle & \\
|f_0(1500)\rangle & \\
|f_0(1710)\rangle &
\end{aligned}
&= \begin{pmatrix} 0.86 & 0.24 & 0.45 \\ -0.45 & -0.06 & 0.89 \\ -0.24 & 0.97 & -0.06 \end{pmatrix} \cdot \begin{aligned}
|n\bar{n}\rangle & \\
|s\bar{s}\rangle & \\
|G\rangle &
\end{aligned} \\
\begin{aligned}
|f_0(1370)\rangle & \\
|f_0(1500)\rangle & \\
|f_0(1710)\rangle &
\end{aligned}
&= \begin{pmatrix} 0.84 & 0.30 & 0.45 \\ -0.40 & -0.21 & 0.89 \\ 0.36 & -0.93 & -0.06 \end{pmatrix} \cdot \begin{aligned}
|1\rangle & \\
|8\rangle & \\
|G\rangle &
\end{aligned}
\end{aligned} \tag{36}$$

$$\begin{aligned}
\begin{aligned}
|f_0(1370)\rangle & \\
|f_0(1500)\rangle & \\
|f_0(1710)\rangle &
\end{aligned}
= \begin{pmatrix} 0.79 & 0.26 & 0.56 \\ -0.58 & 0.02 & 0.81 \\ -0.20 & 0.97 & -0.16 \end{pmatrix} \cdot \begin{aligned}
|n\bar{n}\rangle \\
|s\bar{s}\rangle \\
|G\rangle
\end{aligned} \\
\begin{aligned}
|f_0(1370)\rangle & \\
|f_0(1500)\rangle & \\
|f_0(1710)\rangle &
\end{aligned}
= \begin{pmatrix} 0.80 & 0.24 & 0.56 \\ 0.46 & -0.35 & 0.81 \\ 0.40 & -0.91 & -0.16 \end{pmatrix} \cdot \begin{aligned}
|1\rangle \\
|8\rangle \\
|G\rangle
\end{aligned}
\end{aligned} \tag{37}$$

The common features of these mixing schemes are that the $f_0(1710)$ has a very large $s\bar{s}$ component, while the largest part of the glueball tends to be on the $f_0(1500)$, it is generally split over at least two of the three states. One also sees that the $f_0(1370)$ has the largest SU(3) singlet component.

The other situation is in which the bare glueball comes out heavier than the bare $s\bar{s}$ state. The first of these was carried out by Weingarten and Lee [18]. They computed both the masses of the bare states as well as information on the decay of these states on the lattice. In their model, they had a decay rate that favored heavier quarks, thus enhancing the coupling to the $s\bar{s}$ states. They found the mixing scheme as in equation 38.

$$\begin{aligned}
\begin{aligned}
|f_0(1370)\rangle & \\
|f_0(1500)\rangle & \\
|f_0(1710)\rangle &
\end{aligned}
= \begin{pmatrix} 0.819 & 0.290 & -0.495 \\ -0.399 & 0.908 & -0.128 \\ 0.413 & 0.302 & 0.859 \end{pmatrix} \cdot \begin{aligned}
|n\bar{n}\rangle \\
|s\bar{s}\rangle \\
|G\rangle
\end{aligned} \\
\begin{aligned}
|f_0(1370)\rangle & \\
|f_0(1500)\rangle & \\
|f_0(1710)\rangle &
\end{aligned}
= \begin{pmatrix} 0.836 & 0.236 & -0.495 \\ 0.198 & -0.972 & 0.128 \\ 0.512 & -0.008 & 0.859 \end{pmatrix} \cdot \begin{aligned}
|1\rangle \\
|8\rangle \\
|G\rangle
\end{aligned}
\end{aligned} \tag{38}$$

Giacosa [150] also have two solutions in which the bare glueball mass is heavier than the $s\bar{s}$ mass. For the case of no direct glueball decay, the mixing is given in equation 39, while for the case of the direct glueball decay included, the mixing is given in equation 40.

$$\begin{aligned}
\begin{aligned}
|f_0(1370)\rangle & \\
|f_0(1500)\rangle & \\
|f_0(1710)\rangle &
\end{aligned}
= \begin{pmatrix} 0.81 & 0.19 & 0.54 \\ -0.49 & 0.72 & 0.49 \\ -0.30 & 0.67 & -0.68 \end{pmatrix} \cdot \begin{aligned}
|n\bar{n}\rangle \\
|s\bar{s}\rangle \\
|G\rangle
\end{aligned} \\
\begin{aligned}
|f_0(1370)\rangle & \\
|f_0(1500)\rangle & \\
|f_0(1710)\rangle &
\end{aligned}
= \begin{pmatrix} 0.77 & 0.31 & 0.54 \\ 0.02 & -0.87 & 0.49 \\ 0.14 & -0.72 & -0.68 \end{pmatrix} \cdot \begin{aligned}
|1\rangle \\
|8\rangle \\
|G\rangle
\end{aligned}
\end{aligned} \tag{39}$$

$$\begin{aligned}
\begin{aligned}
|f_0(1370)\rangle & \\
|f_0(1500)\rangle & \\
|f_0(1710)\rangle &
\end{aligned}
= \begin{pmatrix} 0.82 & 0.57 & -0.07 \\ -0.57 & 0.82 & 0.00 \\ -0.06 & 0.04 & -0.99 \end{pmatrix} \cdot \begin{aligned}
|n\bar{n}\rangle \\
|s\bar{s}\rangle \\
|G\rangle
\end{aligned} \\
\begin{aligned}
|f_0(1370)\rangle & \\
|f_0(1500)\rangle & \\
|f_0(1710)\rangle &
\end{aligned}
= \begin{pmatrix} 1.00 & 0.01 & -0.07 \\ 0.01 & -1.00 & 0.00 \\ -0.03 & -0.07 & -0.99 \end{pmatrix} \cdot \begin{aligned}
|1\rangle \\
|8\rangle \\
|G\rangle
\end{aligned}
\end{aligned} \tag{40}$$

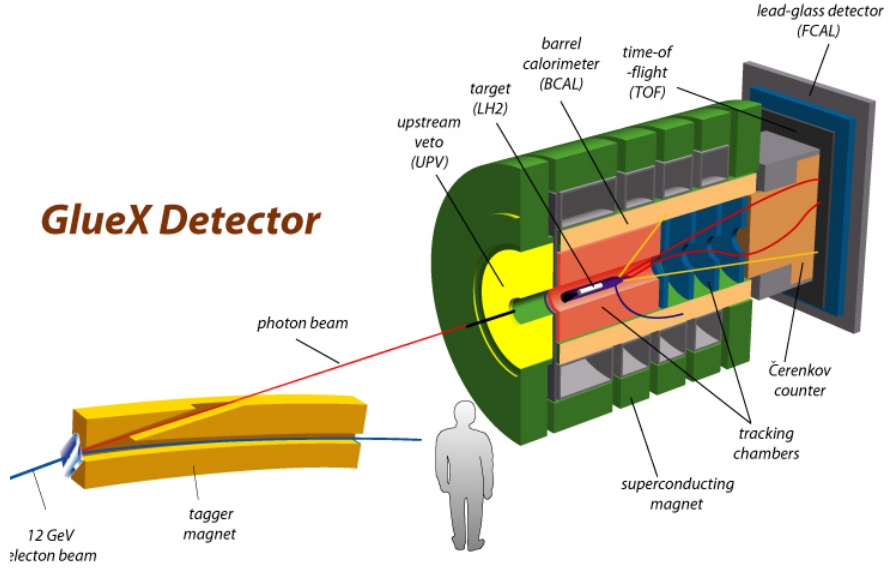


Figure 15: Layout of the GlueX Experiment at Jefferson Laboratory

Finally, Cheng [151] used lattice calculations for the mass of the a_0 the scalar glueball to set the starting values for their fit to the existing data. They also limited the input data on decay rates. In particular, they did not use the strong coupling of the $f_0(1500)$ to $\eta\eta'$ due to the complications of the threshold opening. They find the mixing scheme as given in equation 41.

$$\begin{aligned}
 \begin{pmatrix} |f_0(1370)\rangle \\ |f_0(1500)\rangle \\ |f_0(1710)\rangle \end{pmatrix} &= \begin{pmatrix} 0.78 & 0.51 & -0.36 \\ -0.54 & 0.84 & 0.03 \\ 0.32 & 0.18 & 0.93 \end{pmatrix} \cdot \begin{pmatrix} |n\bar{n}\rangle \\ |s\bar{s}\rangle \\ |G\rangle \end{pmatrix} \\
 \begin{pmatrix} |f_0(1370)\rangle \\ |f_0(1500)\rangle \\ |f_0(1710)\rangle \end{pmatrix} &= \begin{pmatrix} 0.93 & 0.03 & -0.36 \\ 0.04 & -0.99 & 0.03 \\ 0.37 & 0.04 & 0.93 \end{pmatrix} \cdot \begin{pmatrix} |1\rangle \\ |8\rangle \\ |G\rangle \end{pmatrix}
 \end{aligned} \tag{41}$$

A common feature of these latter mixing schemes is that the glueball component ends up mostly in the highest mass state ($f_0(1710)$), while the $f_0(1500)$ comes out being mostly an SU(3) octet and the $f_0(1370)$ is mostly an SU(3) singlet state.

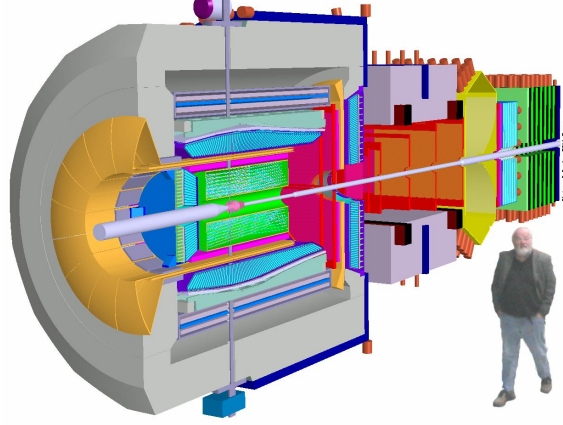


Figure 16: Layout of the PANDA experiment at GSI

6 Planned Experiments

The GlueX Experiment at Jefferson Laboratory

The PANDA Experiment at GSI

The PANDA research program will be conducted at the Facility for Antiproton and Ion Research (FAIR), localized near Frankfurt in Germany. The heart of the new facility is a superconducting synchrotron double-ring facility with a circumference of about 1,100 meters. A system of cooler-storage rings for effective beam cooling at high energies and various experimental halls will be connected to the facility.

At the new FAIR facility, antiproton beams will allow high-precision hadron physics in the upcoming years. A dedicated high-energy storage ring, HESR, will deliver antiproton beams in the momentum range between 1.5 and 15 GeV/ c with unprecedented beam qualities. The energy range has been chosen to allow detailed studies of hadronic systems up to charmonium states. The physics will be done with the PANDA multipurpose detector located inside the HESR. Fig. 16 shows the general layout of the detector. The PANDA collaboration consists of ~ 400 physicists from 48 institutions worldwide.

The general-purpose detector PANDA allows the detection and identification of neutral and charged particles over the relevant angular and energy range. The inner part of the detector can be modified for the needs of individual physics programs. To achieve the physics aims, the detector needs to cover the full solid angle. Good particle identification and excellent energy and angular resolution for charged particles and photons is provided by the following components:

7 Summary

To be written

References

- [1] E. Aker et al. The Crystal Barrel spectrometer at LEAR. *Nucl. Instrum. Meth.*, A321:69–108, 1992.
- [2] Claude Amsler. Proton antiproton annihilation and meson spectroscopy with the Crystal Barrel. *Rev. Mod. Phys.*, 70:1293–1340, 1998.
- [3] Stephen Godfrey and Jim Napolitano. Light meson spectroscopy. *Rev. Mod. Phys.*, 71:1411–1462, 1999.
- [4] F E Close. Gluonic hadrons. *Reports on Progress in Physics*, 51(6):833–882, 1988.
- [5] C. Amsler and N. A. Tornqvist. Mesons beyond the naive quark model. *Phys. Rept.*, 389:61–117, 2004.
- [6] Eberhard Klempt and Alexander Zaitsev. Glueballs, Hybrids, Multiquarks. Experimental facts versus QCD inspired concepts. *Phys. Rept.*, 454:1–202, 2007.
- [7] W. M. Yao *et al.* Review of particle physics. *J. Phys.*, G33:1, 2006.
- [8] Amsler, C., De-Grand, T. and Krusche, B. Review of Particle Physics. *J. Phys.*, G33:165, 2006.
- [9] Claude Amsler and Frank E. Close. Evidence for a scalar glueball. *Phys. Lett.*, B353:385–390, 1995.
- [10] Claude Amsler and Frank E. Close. Is $f_0(1500)$ a scalar glueball? *Phys. Rev.*, D53:295–311, 1996.
- [11] A. Chodos, R. L. Jaffe, K. Johnson, C. B. Thorn, and V. F. Weisskopf. New extended model of hadrons. *Phys. Rev. D*, 9(12):3471–3495, 1974.
- [12] R. L. Jaffe and K. Johnson. Unconventional States of Confined Quarks and Gluons. *Phys. Lett.*, B60:201, 1976.
- [13] Michael S. Chanowitz. RESONANCES IN PHOTON-PHOTON SCATTERING. Presented at 6th Int. Workshop on Photon-Photon Collisions, Lake Tahoe, CA, Sep 10-13, 1984.
- [14] Mariaelena Boglione and M. R. Pennington. Unquenching the scalar glueball. *Phys. Rev. Lett.*, 79:1998–2001, 1997.
- [15] M. R. Pennington, T. Mori, S. Uehara, and Y. Watanabe. Amplitude Analysis of High Statistics Results on $\gamma\gamma \rightarrow \pi^+\pi^-$ and the Two Photon Width of Isoscalar States. 2008.
- [16] Mesut Bahadır Cakir and Glennys R. Farrar. Radiative decay of vector quarkonium: Constraints on glueballs and light gluinos. *Phys. Rev.*, D50:3268–3278, 1994.

- [17] Frank E. Close, Glennys R. Farrar, and Zhen-ping Li. Determining the gluonic content of isoscalar mesons. *Phys. Rev.*, D55:5749–5766, 1997.
- [18] Weon-Jong Lee and D. Weingarten. Scalar quarkonium masses and mixing with the lightest scalar glueball. *Phys. Rev.*, D61:014015, 2000.
- [19] C. Edwards et al. Observation of a Pseudoscalar State at 1440 MeV in J/ψ Radiative Decays. *Phys. Rev. Lett.*, 49:259, 1982.
- [20] J. E. Augustin et al. Radiative Decay of J/ψ into $\eta(1430)$ and Nearby States. *Phys. Rev.*, D42:10–19, 1990.
- [21] D. L. Scharre et al. Observation of the Radiative Transition $\psi \rightarrow \gamma E(1420)$. *Phys. Lett.*, B97:329, 1980.
- [22] C. Amsler and A. Mazoni. Review of Particle Physics. *J. Phys.*, G33:591, 2006.
- [23] S. Spanier and N.A. Tornqvist. Review of Particle Physics. *Phys. Lett.*, B592:506–508, 2004.
- [24] Nathan Isgur and Jack E. Paton. A Flux Tube Model for Hadrons. *Phys. Lett.*, B124:247, 1983.
- [25] Nathan Isgur and Jack E. Paton. A Flux Tube Model for Hadrons in QCD. *Phys. Rev.*, D31:2910, 1985.
- [26] Masaharu Iwasaki, Shin-Ichi Nawa, Takayoshi Sanada, and Fujio Takagi. Flux tube model for glueballs. *Phys. Rev. D*, 68(7):074007, Oct 2003.
- [27] Colin J. Morningstar and Mike J. Peardon. Efficient glueball simulations on anisotropic lattices. *Phys. Rev.*, D56:4043–4061, 1997.
- [28] Ludvig Faddeev, Antti J. Niemi, and Ulrich Wiedner. Glueballs, closed fluxtubes and $\eta(1440)$. *Phys. Rev.*, D70:114033, 2004.
- [29] Y. Koma, H. Suganuma, and H. Toki. Flux-tube ring and glueball properties in the dual ginzburg-landau theory. *Phys. Rev. D*, 60(7):074024, Sep 1999.
- [30] Adam P. Szczepaniak and Eric S. Swanson. The low lying glueball spectrum. *Phys. Lett.*, B577:61–66, 2003.
- [31] Urs M. Heller. SU(3) lattice gauge theory in the fundamental adjoint plane and scaling along the Wilson axis. *Phys. Lett.*, B362:123–127, 1995.
- [32] Christopher Michael and M. Teper. The Glueball Spectrum and Scaling in SU(3) Lattice Gauge Theory. *Phys. Lett.*, B206:299, 1988.

- [33] Christopher Michael and M. Teper. The Glueball Spectrum in SU(3). *Nucl. Phys.*, B314:347, 1989.
- [34] G. S. Bali et al. A Comprehensive lattice study of SU(3) glueballs. *Phys. Lett.*, B309:378–384, 1993.
- [35] J. Sexton, A. Vaccarino, and D. Weingarten. Numerical Evidence for the Observation of a Scalar Glueball. *Phys. Rev. Lett.*, 75:4563–4566, 1995.
- [36] Don Weingarten. Scalar quarkonium and the scalar glueball. *Nucl. Phys. Proc. Suppl.*, 53:232–235, 1997.
- [37] Frank E. Close and Andrew Kirk. Scalar glueball q anti- q mixing above 1-GeV and implications for lattice QCD. *Eur. Phys. J.*, C21:531–543, 2001.
- [38] F. Giacosa, T. Gutsche, and Amand Faessler. A covariant constituent quark/gluon model for the glueball-quarkonia content of scalar-isoscalar mesons. *Phys. Rev.*, C71:025202, 2005.
- [39] Colin J. Morningstar and Mike J. Peardon. The Glueball spectrum from an anisotropic lattice study. *Phys. Rev.*, D60:034509, 1999.
- [40] Y. Chen et al. Glueball spectrum and matrix elements on anisotropic lattices. *Phys. Rev.*, D73:014516, 2006.
- [41] A. Hart and M. Teper. On the glueball spectrum in O(a)-improved lattice QCD. *Phys. Rev.*, D65:034502, 2002.
- [42] Craig McNeile. Hard hadron spectroscopy. *PoS*, LATTICE2007:019, 2007.
- [43] Eric B. Gregory, Alan C. Irving, Craig C. McNeile, Steven Miller, and Zbyszek Sroczynski. Scalar glueball and meson spectroscopy in unquenched lattice QCD with improved staggered quarks. *PoS*, LAT2005:027, 2006.
- [44] A. Abele et al. Test of anti-N N potential models: Isospin relations in anti-p d annihilations at rest and the search for quasinuclear bound states. *Eur. Phys. J.*, C17:583–592, 2000.
- [45] A. Adamo et al. First physics results from OBELIX. *Sov. J. Nucl. Phys.*, 55:1732–1742, 1992.
- [46] P. Salvini et al. anti-p p annihilation into four charged pions at rest and in flight. *Eur. Phys. J.*, C35:21–33, 2004.
- [47] A. Bertin et al. E/ι decays to $K\bar{K}\pi$ in $\bar{p}p$ annihilation at rest. *Phys. Lett.*, B361:187–198, 1995.

- [48] A. Bertin et al. Measurement of the $\eta(1440) \rightarrow K^\pm K_L^0 \pi^\mp$ production rates from $\bar{p}p$ annihilation at rest at three different hydrogen target densities. *Phys. Lett.*, B385:493–499, 1996.
- [49] C. Cicalo et al. Evidence for two pseudoscalar states in the 1.4-GeV to 1.5-GeV mass region. *Phys. Lett.*, B462:453–461, 1999.
- [50] F. Nichitiu et al. Study of the $K^+ K^- \pi^+ \pi^- \pi^0$ final state in anti-proton annihilation at rest in gaseous hydrogen at NTP with the OBELIX spectrometer. *Phys. Lett.*, B545:261–271, 2002.
- [51] A. Bertin et al. Study of the isovector scalar mesons in the channel $\bar{p}p \rightarrow K^\pm K_S^0 \pi^\mp$ at rest with initial angular momentum state selection. *Phys. Lett.*, B434:180–188, 1998.
- [52] M. Bargiotti et al. Coupled channel analysis of $\pi^+ \pi^- \pi^0$, $K^+ K^- \pi^0$ and $K^\pm K_S^0 \pi^\mp$ from $\bar{p}p$ annihilation at rest in hydrogen targets at three densities. *Eur. Phys. J.*, C26:371–388, 2003.
- [53] C. Amsler et al. Coupled channel analysis of $\bar{p}p$ annihilation into $\pi^0 \pi^0 \pi^0$, $\pi^0 \eta \eta$ and $\pi^0 \pi^0 \eta$. *Phys. Lett.*, B355:425–432, 1995.
- [54] C. Amsler et al. High statistics study of $f_0(1500)$ decay into $\pi^0 \pi^0$. *Phys. Lett.*, B342:433–439, 1995.
- [55] C. Amsler et al. Proton - anti-proton annihilation into $\eta \eta \pi$: Observation of a scalar resonance decaying into $\eta \eta$. *Phys. Lett.*, B291:347–354, 1992.
- [56] C. Amsler et al. High statistics study of $f_0(1500)$ decay into $\eta \eta$. *Phys. Lett.*, B353:571–577, 1995.
- [57] C. Amsler et al. $\eta \eta'$ threshold enhancement in $\bar{p}p$ annihilations into $\pi^0 \eta \eta'$ at rest. *Phys. Lett.*, B340:259–263, 1994.
- [58] C. Amsler et al. Protonium annihilation into $K_L^0 K_S^0 \pi^0$ and $K_L^0 K_S^0 \eta$. *Phys. Lett.*, B319:373–380, 1993.
- [59] A. Abele et al. Anti-proton proton annihilation at rest into $K^+ K^- \pi^0$. *Phys. Lett.*, B468:178–188, 1999.
- [60] A. Abele et al. Observation of $f_0(1500)$ decay into $K_L K_L$. *Phys. Lett.*, B385:425–432, 1996.
- [61] A. Abele et al. Study of the $\pi^0 \pi^0 \eta'$ final state in $\bar{p}p$ annihilation at rest. *Phys. Lett.*, B404:179–186, 1997.
- [62] C. Amsler et al. E decay to $\eta \pi \pi$ in $\bar{p}p$ annihilation at rest. *Phys. Lett.*, B358:389–398, 1995.

- [63] A. Abele et al. Study of $\bar{p}p \rightarrow \eta\pi^0\pi^0\pi^0$ at rest. *Nucl. Phys.*, B514:45–59, 1998.
- [64] C. Amsler et al. Observation of a scalar resonance decaying to $\pi^+\pi^-\pi^0\pi^0$ in $\bar{p}p$ annihilation at rest. *Phys. Lett.*, B322:431–440, 1994.
- [65] A. Abele et al. A Study of $f_0(1500)$ decays into $4\pi^0$ in $\bar{p}p \rightarrow 5\pi^0$ at rest. *Phys. Lett.*, B380:453–460, 1996.
- [66] A. Abele et al. Study of f_0 decays into four neutral pions. *Eur. Phys. J.*, C19:667–675, 2001.
- [67] A. Abele et al. 4π decays of scalar and vector mesons. *Eur. Phys. J.*, C21:261–269, 2001.
- [68] A. Abele et al. High mass rho meson states from $\bar{p}d$ annihilation at rest into $\pi^-\pi^0\pi^0 p_{spectator}$. *Phys. Lett.*, B391:191–196, 1997.
- [69] A. Abele et al. $\bar{p}d$ annihilation at rest into $\pi^+\pi^-\pi^- p_{spectator}$. *Phys. Lett.*, B450:275–280, 1999.
- [70] C. Amsler et al. Anti-proton - proton annihilation at rest into $\omega\pi^0\pi^0$. *Phys. Lett.*, B311:362–370, 1993.
- [71] C. Amsler et al. Study of antiproton annihilation on neutrons into $\omega\pi^-\pi^0$. *Nucl. Phys.*, A740:130–146, 2004.
- [72] C. Amsler et al. Study of $K\bar{K}$ resonances in $\bar{p}p \rightarrow K^+K^-\pi^0$ at 900-MeV/c and 1640-MeV/c. *Phys. Lett.*, B639:165–171, 2006.
- [73] A. Abele et al. Observation of resonances in the reaction $\bar{p}p \rightarrow \pi^0\eta\eta$ at 1.94-GeV/c. *Eur. Phys. J.*, C8:67–79, 1999.
- [74] J. Adomeit et al. Evidence for two isospin zero $J^{PC} = 2^{-+}$ mesons at 1645- MeV and 1875-MeV. *Z. Phys.*, C71:227–238, 1996.
- [75] A. Abele et al. Anti-p p annihilation into $\omega\pi^0$, $\omega\eta$ and $\omega\eta'$ at 600-MeV, 1200-MeV and 1940-MeV/c. *Eur. Phys. J.*, C12:429–439, 2000.
- [76] C. Amsler et al. Proton anti-proton annihilation at 900-MeV/c into $\pi^0\pi^0\pi^0$, $\pi^0\pi^0\eta$ and $\pi^0\eta\eta$. *Eur. Phys. J.*, C23:29–41, 2002.
- [77] S. B. Athar et al. Radiative decays of the $\Upsilon(1S)$ to a pair of charged hadrons. *Phys. Rev.*, D73:032001, 2006.
- [78] D. Besson et al. Radiative Decays of the $\Upsilon(1S)$ to $\gamma\pi^0\pi^0$, and $\gamma\eta\eta$ and $\gamma\pi^0\eta$. *Phys. Rev.*, D75:072001, 2007.
- [79] J. Z. Bai et al. The BES upgrade. *Nucl. Instrum. Meth.*, A458:627–637, 2001.

- [80] J. Z. Bai et al. Partial Wave Analysis of $J/\psi \rightarrow \gamma\pi^+\pi^-\pi^+\pi^-$. *Phys. Lett. B*, 472:207, 2000.
- [81] M. Ablikim et al. Partial Wave Analysis of $J/\psi \rightarrow \gamma\pi^+\pi^-$ and $\gamma\pi^0\pi^0$. *Phys. Lett. B*, 642:441, 2006.
- [82] J. Z. Bai et al. Partial Wave Analysis of $J/\psi \rightarrow \gamma K^+K^-$ and $\gamma K_S^0 K_S^0$. *Phys. Rev. D*, 68:052003, 2003.
- [83] M. Ablikim et al. Observation of a near-threshold enhancement in the omega Phi mass spectrum from the doubly OZI suppressed decay $J/\psi \rightarrow \gamma\omega\phi$. *Phys. Rev. Lett.*, 96:162002, 2006.
- [84] M. Ablikim et al. The σ pole in $J/\psi \rightarrow \omega\pi^+\pi^-$. *Phys. Lett. B*, 598:149, 2004.
- [85] M. Ablikim et al. Resonances in $J/\psi \rightarrow \phi\pi^+\pi^-$ and ϕK^+K^- . *Phys. Lett. B*, 607:243, 2005.
- [86] M. Ablikim et al. Study of $J/\psi \rightarrow \omega K^+K^-$. *Phys. Lett. B*, 603:138, 2004.
- [87] S. E. Kopp. The CLEO III detector. *Nucl. Instrum. Meth.*, A384:61–66, 1996.
- [88] D. Cronin-Hennessy et al. Searches for CP violation and pi pi S-wave in the Dalitz-plot of $D^0 \rightarrow \pi^+\pi^-\pi^0$. *Phys. Rev.*, D72:031102, 2005.
- [89] G. Bonvicini et al. Dalitz plot analysis of the $D^+ \rightarrow \pi^+\pi^+\pi^-$ decay. *Phys. Rev.*, D76:012001, 2007.
- [90] K. Benslama et al. Anti-search for the glueball candidate $f(J)(2220)$ in two-photon interactions. *Phys. Rev.*, D66:077101, 2002.
- [91] Frank E. Close and Andrew Kirk. Large isospin mixing in Phi radiative decay and the spatial size of the $f_0(980)$ - $a_0(980)$ meson. *Phys. Lett.*, B515:13–16, 2001.
- [92] D. Robson. A Basic Guide for the Glueball Spotter. *Nucl. Phys.*, B130:328, 1977.
- [93] A. Kirk. A glueball $q\bar{q}$ filter in central production. 1999.
- [94] T. A. Armstrong et al. Study of the centrally produced pi pi and K anti-K systems at 85-GeV/c and 300-GeV/c. *Z. Phys.*, C51:351–364, 1991.
- [95] F. Binon et al. Hodoscope Multi - Photon Spectrometer Gams-2000. *Nucl. Instrum. Meth.*, A248:86, 1986.
- [96] D. Alde et al. Acquisition System For The Hodoscope Spectrometer Gams-4000. *Nucl. Instrum. Meth.*, A240:343, 1985.
- [97] S. Abatzis et al. A further study of the centrally produced $\pi^+\pi^-$ and $\pi^+\pi^-\pi^+\pi^-$ channels in pp interactions at 300 and 450 GeV/c. *Phys. Lett.*, B353:589–594, 1995.

- [98] D. Barberis et al. A study of the centrally produced $\pi^+\pi^-\pi^+\pi^-$ channel in pp interactions at 450-GeV/c. *Phys. Lett.*, B413:217–224, 1997.
- [99] D. Barberis et al. A spin analysis of the 4π channels produced in central pp interactions at 450-GeV/c. *Phys. Lett.*, B471:440–448, 2000.
- [100] D. Barberis et al. A study of the $f_0(1370)$, $f_0(1500)$, $f_0(2000)$ and $f_2(1950)$ observed in the centrally produced 4π final states. *Phys. Lett.*, B474:423–426, 2000.
- [101] D. Barberis et al. A partial wave analysis of the centrally produced $\pi^0\pi^0$ system in pp interactions at 450-GeV/c. *Phys. Lett.*, B453:325–332, 1999.
- [102] D. Barberis et al. A partial wave analysis of the centrally produced $\pi^+\pi^-$ system in pp interactions at 450-GeV/c. *Phys. Lett.*, B453:316–324, 1999.
- [103] D. Barberis et al. A partial wave analysis of the centrally produced K^+K^- and $K_S^0K_S^0$ systems in pp interactions at 450-GeV/c and new information on the spin of the $f_J(1710)$. *Phys. Lett.*, B453:305–315, 1999.
- [104] D. Barberis et al. A coupled channel analysis of the centrally produced K^+K^- and $\pi^+\pi^-$ final states in pp interactions at 450-GeV/c. *Phys. Lett.*, B462:462–470, 1999.
- [105] D. Barberis et al. A study of the $\eta\eta'$ and $\eta'\eta'$ channels produced in central pp interactions at 450-GeV/c. *Phys. Lett.*, B471:429–434, 2000.
- [106] D. Barberis et al. A study of the $\eta\eta$ channel produced in central pp interactions at 450-GeV/c. *Phys. Lett.*, B479:59–66, 2000.
- [107] D. Barberis et al. A study of the centrally produced $\phi\phi$ system in pp interactions at 450-GeV/c. *Phys. Lett.*, B432:436–442, 1998.
- [108] D. Barberis et al. A study of the $\omega\omega$ channel produced in central pp interactions at 450-GeV/c. *Phys. Lett.*, B484:198–204, 2000.
- [109] D. Barberis et al. A study of the centrally produced $K^*(892)\bar{K}^*(892)$ and $\phi\omega$ systems in pp interactions at 450-GeV/c. *Phys. Lett.*, B436:204–210, 1998.
- [110] D. Barberis et al. A study of the centrally produced $\pi^0\pi^0\pi^0$ channel in pp interactions at 450-GeV/c. *Phys. Lett.*, B507:14–18, 2001.
- [111] D. Barberis et al. A study of the centrally produced $\pi^+\pi^-\pi^0$ channel in pp interactions at 450-GeV/c. *Phys. Lett.*, B422:399–404, 1998.
- [112] D. Barberis et al. A study of the centrally produced $\eta\pi^0$ and $\eta\pi^-$ systems in pp interactions at 450-GeV/c. *Phys. Lett.*, B488:225–233, 2000.
- [113] D. Barberis et al. A study of the $\eta\pi^+\pi^-$ channel produced in central pp interactions at 450-GeV/c. *Phys. Lett.*, B471:435–439, 2000.

- [114] D. Barberis et al. A study of the $K\bar{K}\pi$ channel produced centrally in pp interactions at 450-GeV/c. *Phys. Lett.*, B413:225–231, 1997.
- [115] R. Ahohe et al. The search for $\eta(1440) \rightarrow K^0(S) K^+ \pi^-$ in two-photon fusion at CLEO. *Phys. Rev.*, D71:072001, 2005.
- [116] D. Decamp et al. ALEPH: A DETECTOR FOR ELECTRON - POSITRON ANNIHILATIONS AT LEP. *Nucl. Instrum. Meth.*, A294:121–178, 1990.
- [117] THE CONSTRUCTION OF THE L3 EXPERIMENT. *Nucl. Instrum. Meth.*, A289:35–102, 1990.
- [118] M. Acciarri et al. $K_S^0 K_S^0$ final state in two photon collisions and implications for glueballs. *Phys. Lett.*, B501:173–182, 2001.
- [119] M. Acciarri et al. Light resonances in $K_S^0 K^\pm \pi^\mp$ and $\eta \pi^+ \pi^-$ final states in $\gamma\gamma$ collisions at LEP. *Phys. Lett.*, B501:1–11, 2001.
- [120] R. Barate et al. Search for the glueball candidates $f_0(1500)$ and $f_J(1710)$ in gamma gamma collisions. *Phys. Lett.*, B472:189–199, 2000.
- [121] D. Aston et al. THE STRANGE MESON RESONANCES OBSERVED IN THE REACTION $K^- p \rightarrow \text{anti-}K^0 \pi^+ \pi^- n$ AT 11-GeV/c. *Nucl. Phys.*, B292:693, 1987.
- [122] S. I. Bityukov et al. Observation of resonance with mass $M = 1814\text{-MeV}$, decaying into $\pi^- \eta \eta$. *Phys. Lett.*, B268:137–141, 1991.
- [123] Z. Bar-Yam et al. A cylindrical drift chamber with azimuthal and axial position readout. *Nucl. Instrum. Meth.*, A386:235–248, 1997.
- [124] R. R. Crittenden et al. A 3000 element lead-glass electromagnetic calorimeter. *Nucl. Instrum. Meth.*, A387:377–394, 1997.
- [125] S. Devons et al. OBSERVATIONS OF $\text{anti-}p p \rightarrow 3 \pi^0, 2 \pi^0 \eta^0$ AT REST. *Phys. Lett.*, B47:271, 1973.
- [126] L. Gray, T. Kalogeropoulos, A. Nandy, J. Roy, and S. Zenone. EVIDENCE FOR A $\pi^+ \pi^-$ ISOSCALAR RESONANCE DEGENERATE WITH THE F' PRODUCED IN $\text{ANTI-}p n$ ANNIHILATIONS AT REST. *Phys. Rev.*, D27:307–310, 1983.
- [127] F. G. Binon et al. $G(1590)$: A Scalar Meson Decaying Into Two η Mesons. *Nuovo Cim.*, A78:313, 1983.
- [128] F. G. Binon et al. STUDY OF $\pi^- p \rightarrow \eta' \eta n$ IN A SEARCH FOR GLUEBALLS. *Nuovo Cim.*, A80:363, 1984.
- [129] M. Strohmeier-Presicek, T. Gutsche, Amand Faessler, and R. Vinh Mau. 4π decay modes of the $f_0(1500)$ resonance. *Phys. Lett.*, B438:21–26, 1998.

- [130] M. Gaspero. Evidence for the dominance of an $I(G) J(PC) = 0+0++$ resonance in $\text{anti-p } n \rightarrow 2 \text{ pi}^+ 3 \text{ pi}^-$ annihilation at rest. *Nucl. Phys.*, A562:407–445, 1993.
- [131] C. Edwards et al. Observation of an eta eta Resonance in J/psi Radiative Decays. *Phys. Rev. Lett.*, 48:458, 1982.
- [132] Donald E. Groom et al. Review of particle physics. *Eur. Phys. J.*, C15:1–878, 2000.
- [133] A. Kirk. Resonance production in central p p collisions at the CERN Omega spectrometer. *Phys. Lett.*, B489:29–37, 2000.
- [134] F. Antinori et al. A Further study of the centrally produced $\text{pi}^+ \text{pi}^-$ and $\text{pi}^+ \text{pi}^- \text{pi}^+ \text{pi}^-$ channels in p p interactions at 300-GeV/c and 450-GeV/c. *Phys. Lett.*, B353:589–594, 1995.
- [135] Chang-Zheng Yuan. Hadron spectroscopy from BES and CLEOc. *AIP Conf. Proc.*, 814:65–77, 2006.
- [136] C. Amsler et al. Review of particle physics. *Phys. Lett.*, B667:1, 2008.
- [137] J. Z. Bai et al. Studies of xi (2230) in J / psi radiative decays. *Phys. Rev. Lett.*, 76:3502–3505, 1996.
- [138] J. Z. Bai et al. Experimental study of J/psi radiative decay to $\text{pi}^0 \text{pi}^0$. *Phys. Rev. Lett.*, 81:1179–1182, 1998.
- [139] R. M. Baltrusaitis et al. Observation of a Narrow K anti-K State in J/psi Radiative Decays. *Phys. Rev. Lett.*, 56:107, 1986.
- [140] J. E. Augustin et al. RADIATIVE DECAY OF J / psi INTO gamma $\text{pi}^+ \text{pi}^-$. *Z. Phys.*, C36:369–376, 1987.
- [141] D. Alde et al. 2.22-GeV eta eta-prime STRUCTURE OBSERVED IN 38-GeV/c AND 100-GeV/c $\text{pi}^- \text{p}$ COLLISIONS. *Phys. Lett.*, B177:120, 1986.
- [142] A. Hasan and D. V. Bugg. A search for the xi(2235) in $\text{anti-p } p \rightarrow \text{pi}^- \text{pi}^+$. *Phys. Lett.*, B388:376–379, 1996.
- [143] G. Bardin et al. SEARCH FOR A NARROW RESONANCE ABOUT THE xi (2230) IN THE FORMATION CHANNEL $\text{anti-p } p \rightarrow K^+ K^-$. *Phys. Lett.*, B195:292, 1987.
- [144] J. Sculli, J. H. Christenson, G. A. Kreiter, P. Nemethy, and P. Yamin. LIMITS ON XI (2.2) FORMATION IN $\text{ANTI-P } P \rightarrow K^+ K^-$. *Phys. Rev. Lett.*, 58:1715–1718, 1987.
- [145] C. Evangelista et al. Measurement of the $\text{anti-p } p \rightarrow K(S) K(S)$ reaction from 0.6-GeV/c to 1.9-GeV/c. *Phys. Rev.*, D56:3803–3810, 1997.

- [146] C. Evangelista et al. Study of the reaction $\text{anti-p p} \rightarrow \bar{\chi} \text{Phi Phi}$ from 1.1-GeV/c to 2.0-GeV/c. *Phys. Rev.*, D57:5370–5381, 1998.
- [147] A. Buzzo et al. Search for narrow anti-p p resonances in the reaction $\text{anti-p p} \rightarrow \bar{\chi} \text{anti-p p pi}^+ \text{pi}^-$. *Z. Phys.*, C76:475–478, 1997.
- [148] K. K. Seth. A high resolution search for the tensor glueball. *Nucl. Phys.*, A663:600–605, 2000.
- [149] F. Buccella, Maurizio Lusignoli, and A. Pugliese. Charm nonleptonic decays and final state interactions. *Phys. Lett.*, B379:249–256, 1996.
- [150] F. Giacosa, Th. Gutsche, V. E. Lyubovitskij, and Amand Faessler. Scalar nonet quarkonia and the scalar glueball: Mixing and decays in an effective chiral approach. *Phys. Rev.*, D72:094006, 2005.
- [151] Hai-Yang Cheng, Chun-Khiang Chua, and Keh-Fei Liu. Scalar glueball, scalar quarkonia, and their mixing. *Phys. Rev.*, D74:094005, 2006.